Erwin Zehe ; Günter Blöschl

Predictability of hydrologic response at the plot and catchment scales: Role of initial conditions

first published in:
Water Resources Research (2004) 40, W10202

Postprint published at the Institutional Repository of the Potsdam University:
In: Postprints der Universität Potsdam
Mathematisch-Naturwissenschaftliche Reihe ; 166
http://opus.kobv.de/ubp/volltexte/2012/6011/
http://nbn-resolving.de/urn:nbn:de:kobv:517-opus-60119

Postprints der Universität Potsdam
Mathematisch-Naturwissenschaftliche Reihe ; 166

Predictability of hydrologic response at the plot and catchment scales: Role of initial conditions

Erwin Zehe
Institute of Geoecology, University of Potsdam, Potsdam, Germany

Günter Blöschl
Institute of Hydraulics, Hydrology and Water Resources Management, Vienna University of Technology, Vienna, Austria

Received 7 November 2003; revised 1 April 2004; accepted 12 August 2004; published 1 October 2004.

[1] This paper examines the effect of uncertain initial soil moisture on hydrologic response at the plot scale (1 m^2) and the catchment scale (3.6 km^2) in the presence of threshold transitions between matrix and preferential flow. We adopt the concepts of microstates and macrostates from statistical mechanics. The microstates are the detailed patterns of initial soil moisture that are inherently unknown, while the macrostates are specified by the statistical distributions of initial soil moisture that can be derived from the measurements typically available in field experiments. We use a physically based model and ensure that it closely represents the processes in the Weiherbach catchment, Germany. We then use the model to generate hydrologic response to hypothetical irrigation events and rainfall events for multiple realizations of initial soil moisture microstates that are all consistent with the same macrostate. As the measures of uncertainty at the plot scale we use the coefficient of variation and the scaled range of simulated vertical bromide transport distances between realizations. At the catchment scale we use similar statistics derived from simulated flood peak discharges. The simulations indicate that at both scales the predictability depends on the average initial soil moisture state and is at a minimum around the soil moisture value where the transition from matrix to macropore flow occurs. The predictability increases with rainfall intensity. The predictability increases with scale with maximum absolute errors of 90 and 32% at the plot scale and the catchment scale, respectively. It is argued that even if we assume perfect knowledge on the processes, the level of detail with which one can measure the initial conditions along with the nonlinearity of the system will set limits to the repeatability of experiments and limits to the predictability of models at the plot and catchment scales. *INDEX TERMS:* 1866 Hydrology: Soil moisture; 1860 Hydrology: Runoff and streamflow; 1875 Hydrology: Unsaturated zone; *KEYWORDS:* flood response, hydrological model, predictability, preferential flow, scale

Citation: Zehe, E., and G. Blöschl (2004), Predictability of hydrologic response at the plot and catchment scales: Role of initial conditions, *Water Resour. Res.*, *40*, W10202, doi:10.1029/2003WR002869.

1. Introduction

[2] Understanding and modeling hydrologic system response at different scales is hampered by an often poor reproducibility of plot-scale and catchment-scale experiments. The same set of measured parameters, state variables and boundary conditions can often be associated with markedly different system responses. *Lischeid et al.* [2000], for example, observed tracer velocities between 30.6 and 10.6 m d^{-1} during three identical steady state field-scale breakthrough experiments at the Gårdsjön test catchment. The differences could not be related to any measurable difference in the experimental conditions. Investigating field-scale tracer transport, *Lennartz et al.* [1999] showed that for their highly macroporous soil it was not possible to predict whether preferential flow will occur or not, even though they had obtained very detailed measurements of soil parameters and the moisture state. When one moves up to larger scales the same problem prevails. As lucidly discussed by *Beven* [2000], no matter what is the sophistication of a physically based model there will always be a large degree of uncertainty in the predictions which will be difficult to account for. This uncertainty limits the predictability of hydrologic response.

[3] There have been a number of alternative explanations for the sources of this uncertainty in the hydrologic literature over the years. These include parameter uncertainty [*Wood*, 1976], uncertainty in the model structure [*Beven*, 1989], and uncertainty in the input data and initial conditions [*Grayson and Blöschl*, 2000]. A recent workshop report on challenges in hydrologic predictability noted [*National Research Council* (*NRC*), 2003, p. 17] ''in watershed rainfall-runoff transformation...initial and boundary conditions are the critical issues.'' This variable assessment raises an interesting question of whether the detailed measurements typically available in research catchments would constrain the system state enough to give

0043-1397/04/2003WR002869$09.00

unique predictions of hydrologic response, assuming perfect knowledge on the nature of the processes (as represented by the structure and parameters of a model). Clearly, this will depend on the level of detail of the field measurements but, no matter how detailed the measurements are, there will always be points in space where we do not have measurements, so there will always be a smaller-scale component of hydrologic variability that will not be captured by the data. This small-scale component may or may not become important in controlling hydrologic response. This is the uncertainty this paper examines with a focus on initial conditions.

[4] The degree to which field measurement constrain the catchment state in terms of producing a unique response will also depend on the degree and type of nonlinearity of the underlying processes. Certain types of nonlinearity lead to chaotic behavior of the system which amplifies uncertainties and limits predictability significantly [*Gleick*, 1993; *Sivakumar*, 2000]. In this paper we examine threshold behavior which is one particular form of process nonlinearity. There are a number of threshold processes in hydrology where the system switches between different "dynamic regimes." An obvious example of two different regimes is wet and dry periods of rainfall. Similarly, evaporation may be subject to different regimes, either controlled by atmospheric demand or by soil hydraulic properties [*Dooge*, 1986]. Snowmelt and freezing are typical threshold processes. Another example is surface runoff generation which is often conceptualized as a threshold process. If rainfall intensity exceeds infiltration capacity surface runoff will occur or, alternatively, if soil saturation is reached, surface runoff will also occur. *Grayson et al.* [1997] observed two regimes of catchment behavior, one being the wet state which is dominated by lateral water movement through both surface and subsurface paths, and the other being the dry state which is dominated by vertical fluxes that are controlled by soil properties and local terrain characteristics. Another important example of a threshold process is the switch between well mixed matrix flow and preferential flow paths in the subsurface [*Flury et al.*, 1994].

[5] While numerous studies have identified the presence of threshold transitions in hydrology, both in the context of preferential flow and other processes, the degree of uncertainty in the system output imparted by the threshold behavior, to our knowledge, has not been dealt with in the literature before. Furthermore, there is an important scale issue involved, both in the level of detail field observations can capture small-scale variability and in the representation of threshold processes. When one moves up in scale one would expect the nonlinear behavior to "average out" and the processes to behave more linearly as suggested by the central limit theorem [*Sivapalan and Wood*, 1986]. The small-scale variability not captured by the data may hence introduce less uncertainty than at smaller scales. However, if nonrandom, structured patterns in the media characteristics and/or the soil moisture state exist, only part of this nonlinearity may average out, if at all [*Blöschl and Sivapalan*, 1995]. Whether the uncertainty due to nonlinearity decreases with scale, or not, so far is not clear.

[6] The aim of this paper therefore is to examine two questions: First, what is the predictability of a hydrologic response by a model constrained by typically available field data of the catchment state, assuming perfect knowledge on the nature of the processes? Second, what are the factors that control the predictability, and does it change when moving from the plot scale to the catchment scale? We will illustrate these more general issues for the case of infiltration where processes may switch between matrix and preferential flow, and catchment runoff where processes may switch between runoff generation processes. We will focus on the role of antecedent soil moisture. The analysis in this paper is based on Monte Carlo simulations (compare section 5) using a physically based hydrologic model (compare section 4.1). Unlike most of the previous studies that were based on hypothetical scenarios [e.g., *Russo et al.*, 1994; *Tsang et al.*, 1996], the simulations in this paper are based on very detailed field data. These are used (1) to ensure that the model closely portrays real system response both at the plot and catchment scales (compare sections 4.2.3 and 4.3.3) and (2) to define the soil moisture variability in a realistic way (compare sections 4.2.2 and 4.3.2). The paper is organized as follows. We first discuss the notion of microstates and macrostates. We next summarize the experimental setup, and give a brief outline of the CATFLOW model which is used both at the plot and the catchment scales. We then describe the methods of generating uncertain initial soil moisture states and the spatial distribution of soil properties, and demonstrate that the model works well at both scales. In the next sections we present the results of the Monte Carlo study that focuses on infiltration at the plot scale (section 5.1) and runoff generation at the catchment (section 5.2) scale and discuss our findings in the light of the recent literature.

2. Microstates and Macrostates and Hydrologic Predictability

[7] This paper deals with the inherent uncertainty of observed initial conditions and the propagation of this uncertainty to hydrologic response in a nonlinear system. At the catchment scale it is not possible to fully measure the initial conditions of the soil. If we go down in scale, to the plot scale, we are able to collect more detailed data but no matter what the spatial resolution of the measurements is, there will always be some fine-scale detail not captured by the measurements. This fine-scale detail may or may not matter for making hydrologic predictions at the plot and catchment scales. In hydrology very little attention has been devoted to this issue in the past. There has been some work on the level of detail necessary to represent the important features of runoff response prompted by the representative area (REA) concept of *Wood et al.* [1988]. The idea of this research was that, at a certain scale, the small-scale hydrologic variability may average out and this is a convenient scale for a model element size, as the model equations are likely to be less scale dependent than for other element sizes. *Blöschl et al.* [1995] showed that, while this is a useful and thought provoking concept, it may not be possible to find a single value of an REA as the scale at which processes average out very much depends on the type of process. This type of scale research, however, did not address the issue of predictability. To address this question, in this paper we adopt concepts from statistical mechanics [*Boltzmann*, 1995; *Landau and Lifshitz*, 1999].

Table 1. Definition of Microstates and Macrostates of Initial Soil Moisture at the Plot and Catchment Scales

	Plot Scale	Catchment Scale
Microstate	spatial pattern (2-D vertical)	spatial pattern (2-D horizontal)
Macrostate	first and second moments	first and second moments, variogram, point data

[8] In statistical mechanics there is a similar problem of uncertain initial conditions as in hydrology. According to *Tolman* [1979, p. 1], ''The principles of ordinary mechanics may be regarded as allowing us to make precise predictions as to the future state of a mechanical system from a precise knowledge of its initial state. On the other hand, the principles of statistical mechanics are to be regarded as permitting us to make reasonable predictions as to the future condition of a system, which may be expected to hold on the average, starting from an incomplete knowledge of its initial state.'' The knowledge of the initial state of soil moisture is certainly incomplete in the case of catchment hydrology. Following the concepts of statistical mechanics, let us consider the kinetic energy of a mol of a gas. The gas can be described in greatest detail by specifying its microscopic state, or microstate, at any time, i.e., the exact values of the kinetic energy of each of the 10^{23} individual molecules. However, it is impossible to measure this microscopic state and we may not be interested in the full detail on the behavior of each and every molecule either. Instead, it may be possible to measure the macroscopic state or macrostate of the gas represented by average quantities or distributions. One such macroscopic quantity is the gas temperature which is a measure of the average kinetic energy of the gas molecules. It is impossible to measure the microstate but it is possible to measure the macrostate. The macrostate characterizes the microscopic reality in a statistical and therefore uncertain sense. A set of numerous possible microstates is consistent with the same macrostate. This is often referred to as a ''degradation'' of the measurable macrostate into a set of possible microstates.

[9] In this paper we use the concepts of microstates and macrostates for specifying initial soil moisture both at the plot and catchment scales. The microstates are the detailed patterns of soil moisture while the macrostates are specified by the statistical distributions of soil moisture obtained from measurements as typically available in detailed research catchment studies. At the plot scale we define the microstate of a soil as the detailed two-dimensional (vertical) pattern of soil moisture over a profile of about 1×1 m^2. The microstate is not observable but we can measure soil moisture at individual points from which we can infer the distribution function of soil moisture. We measured soil moisture at two 4 m^2 plots at 25 points each by time domain reflectometry (TDR). We then specified the macrostate of soil moisture by the first two moments of the spatial distribution derived from these point measurements (Table 1). At the catchment scale we define the microstate of the soil as the detailed two-dimensional (horizontal) pattern of soil moisture over a 3.6 km^2 catchment. Again, the microstate is not observable but we can measure soil moisture at individual points from which we can infer the distribution function of soil moisture. We measured soil moisture at 61 points within the catchment, again using TDR. We specified the macrostate of soil moisture by the first two moments of the spatial distribution and the spatial correlation or variogram (derived from the point measurements), and by the values of soil moisture at each of the 61 points (Table 1). At the catchment scale the description of the macrostate of soil moisture is more detailed than that at the plot scale as, in addition to the univariate moments, the variogram and values at individual points are specified. We argue that this is a typical setup in a research catchment. At the plot scale, disturbances of the soil by the measurements are more problematic than at the catchment scale. Because of this, in the plot-scale measurements of this paper, we did not measure soil moisture in profiles but in a horizontal plane on plots adjacent to the irrigation sites. We were therefore not in the position to derive a vertical variogram, nor were we in the position to use the individual point measurements at their exact locations for specifying the macrostate of soil moisture at the plot scale.

[10] We then perform Monte Carlo simulations of infiltration events at the plot scale (compare section 5.1) and Monte Carlo simulations of runoff events at the catchment scale (compare section 5.2). At both scales we generate multiple realizations of soil moisture patterns, each pattern representing one possible microstate (compare sections 4.2.2 and 4.3.2). All the realizations (or microstates) are consistent with the macrostate of soil moisture derived from the field measurements. In other words we assume that the macrostate is known while the microstate is unknown. The lack of knowledge on the microstate of soil moisture introduces uncertainty into the system. We analyze this uncertainty by using the soil moisture microstates as the initial conditions of a physically based hydrologic model in the Monte Carlo simulations at both scales. The variability in infiltration (at the plot scale) and flood runoff (at the catchment scale) between the realizations is then used as a measure of the uncertainty in hydrologic response introduced by uncertain initial soil moisture (compare sections 5.1 and 5.2). These multiple realizations can be interpreted as multiple hypothetical experiments. If, for a given rainfall forcing, we measured soil moisture and hydrologic response many times, the relationship between the two most likely will not be unique, as the uncertainty in initial soil moisture limits the predictability of hydrologic response. The limits of predictability of hydrologic response may hence be interpreted as the limits to the reproducibility of hydrologic experiments. This is what is quantified in the simulations in this paper.

[11] In the analyses of this paper we examine a single source of uncertainty, i.e., initial soil moisture and assume that the effects of other sources such as model structure, model parameters and inputs are small. It is clear that the other sources will degrade the predictability beyond the results of this paper. We also assume that the local measurement error of soil moisture is not large as compared to the uncertainty of the microstate. At the plot scale the measurement error was 0.01 as compared to a spatial variance of 0.02 m^3 m^{-3}. At the catchment scale the measurement error was 0.01 as compared to a small-scale variance not captured by the measurement of 0.2 m^3 m^{-3}. At both scales the measurement error was accounted for in

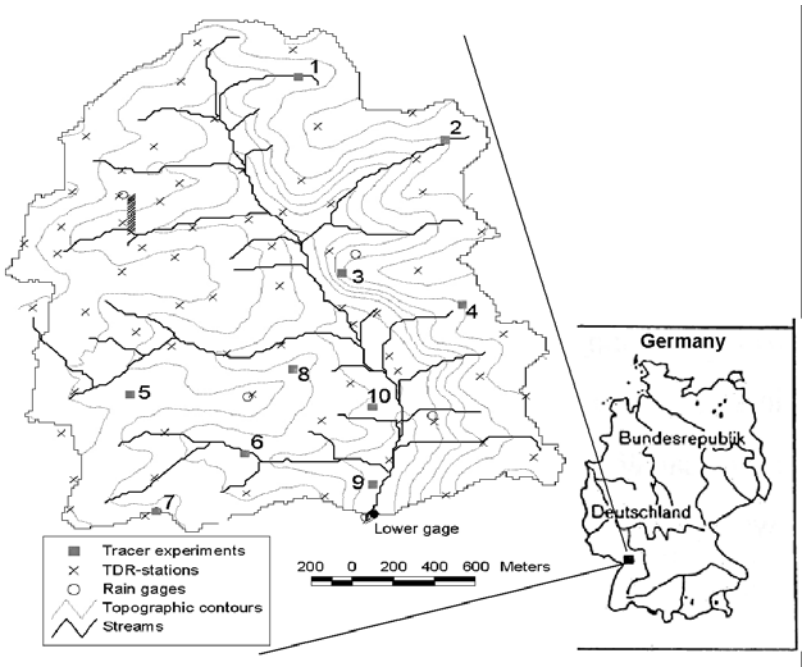

Figure 1. Observational network of the Weiherbach catchment. The field sites of the plot-scale irrigation tracer experiments are indicated by solid rectangles and numbers. Soil moisture was measured at 61 TDR stations at weekly intervals (crosses). Topographic contour interval is 10 m.

the generation of the microstates of soil moisture, as the variance used consisted of both the measurement error and true spatial variance.

3. Catchment and Experiments

3.1. Hydrologic Setting of the Experiments

[12] The Monte Carlo simulations are based on detailed laboratory data and field observations that were conducted in the Weiherbach valley [*Zehe et al.*, 2001]. The Weiherbach valley is a rural catchment of 3.6 km^2 size situated in a Loess area in the south west of Germany. Geologically it consists of Keuper and Loess layers of up to 15 m thickness. The climate is semi humid with an average annual precipitation of 750–800 mm yr^{-1}, average annual runoff of 150 mm yr^{-1}, and annual potential evapotranspiration of 775 mm yr^{-1}.

[13] More than 95% of the total catchment area are used for cultivation of agricultural crops or pasture, 4% are forested and 1% is paved area. Crop rotation is usually ounce a year. Typical main crops are barely or winter barely, corn, sunflowers, turnips, and peas, typical intermediate crops are mustard or clover. Plowing is usually to a depth of 30 to 35 cm in early spring or early fall, depending on the cultivated crop. A few locations in the valley floor are tile drained in a depth of approximately 1 m. However, the total portion of tile drained area is less than 0.5% of the total catchment.

[14] Most of the Weiherbach hillslopes exhibit a typical Loess catena with the moist but drained Colluvisols located at the hill foot and dryer Calcaric Regosols located at the top and mid slope sector. Preferential pathways in the Weiherbach soils are very apparent. They are mainly a result of earthworm burrows and their spatial pattern is closely related to the typical hillslope soil catena. The preferential pathways, or macropores, enhance infiltration and decrease storm runoff as storm runoff only consists of surface runoff in this type of landscape. The detailed field observations [*Zehe et al.*, 2001] in the Weiherbach catchment indicated that storm runoff is produced by infiltration excess overland flow. Because of the small portion of tile rained areas, runoff from tile drains is of minor importance for catchment-scale runoff response. Any water that infiltrates into the soil percolates into the deep loess layer. A bromide tracer experiment conducted over 2 years on an entire hillslope in the catchment suggested that there is very little lateral flow in the soils. There is an aquifer at the base of the loess layer. The tracer experiments also indicated that the travel time for the infiltrating water to reach the aquifer is likely more than 10 years. As a result of these mechanisms, event runoff coefficients are small. The runoff coefficient for the largest event on record was 0.13.

3.2. Plot-Scale Experiments and Macrostates

3.2.1. Outline of Experimental Procedure

[15] A series of 10 plot-scale tracer experiments was conducted in summer 1996 [*Zehe and Flühler*, 2001b]; the location of the field site is shown in Figure 1. All experiments were carried out under similar conditions in terms of irrigation rate and amount, tracer concentration and extraction of soil samples. 1.4 × 1.4 m plots were irrigated over 2 hours using 25 mm of a tracer mix consisting of Brilliant Blue to stain flow patterns and bromide (Br^-) as a conservative tracer. Two vertical soil profiles were excavated one day after the start of the irrigation. 10 × 10 × 10 cm^3 soil samples were extracted from each stained cell of the sampling grid and 10 cm below the leading edge of the dye pattern and analyzed for their bromide content. Some sites showed evidence of strongly preferential flow while others showed evidence of matrix flow. The dye flow patterns of a site exhibiting strongly preferential flow (site 10) is shown

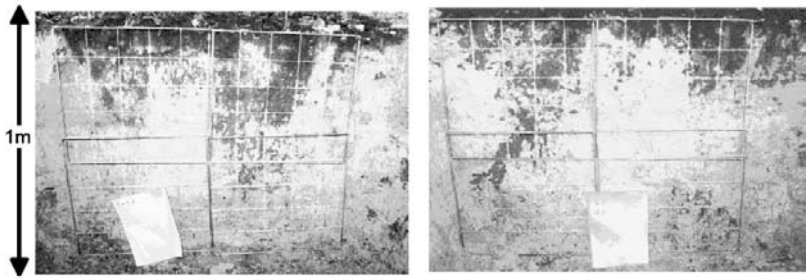

Figure 2. Dye flow patterns observed 1 day after irrigation in two vertical soil profiles at site 10 (see Figure 1). The 10 × 10 cm sampling grid for bromide samples is shown.

in Figure 2 as an example. Site 10 is located close to the Weiherbach creek in a highly macroporous Colluvisol (Figure 1). To characterize the flow regime of preferential versus matrix flow we computed for each 10 × 10 × 100 cm^3 column the distance of the bromide center of mass from the ground surface, z_c. For each site we then calculated the average depth $\bar{z}_c$ of the z_c of all columns of the two profiles as well as their standard deviation σ_c. Figure 3 shows σ_c plotted against $\bar{z}_c$ for each site as well as a typical tracer pattern from each group. Visual inspection of the bromide tracer and simultaneous dye patterns showed that on the basis of this diagram the tracer patterns can be classified into groups of similar behavior. Group 1 (squares in Figure 3) consists of matrix flow patterns, group 2 (circles in Figure 3) consists of preferential flow patterns and group 3 (diamonds in Figure 3) consists of strongly preferential flow patterns. As can be seen from Figure 3, matrix flow dominated tracer patterns are associated with much smaller values of $\bar{z}_c$ and σ_c than the preferential flow patterns. These statistical parameters appear to be a good measure of the presence or absence of preferential flow and will therefore be used to characterize simulated flow patterns on the plot scale in this paper. In the following, the parameters $\bar{z}_c$ and σ_c will be referred to as the average and the variation of the bromide transport distance, respectively.

3.2.2. Measurement of Soil Moisture Macrostate and Soil Properties

[16] In order to determine the hydraulic properties of the soil matrix and the local macropore system as well as to measure initial soil moisture in a representative way, we conducted additional measurements on 4 separate plots of 4 m^2 size each that were located close to the irrigation site 10. At two of them the initial soil moisture was measured in a horizontal plane in the upper 15 cm of the soil using TDR probes at 25 points. The measurements were taken at the same time as the irrigation experiment was performed on site 10. Each point measurement was repeated 5 times. The average and the spatial standard deviation of soil moisture at the two plots were 0.271 ± 0.02 $m^3\ m^{-3}$ and 0.2695 ± 0.02 $m^3\ m^{-3}$, respectively. Using the 5 repetitions at each point the measurement error was estimated as 0.01 $m^3\ m^{-3}$. As the average and the standard deviation of the soil moisture at the two plots match within the measurement error, we can assume that they are representative of the macrostate of the initial soil moisture pattern at the irrigation plot in the above specified sense.

[17] At the two other plots (termed plots 1 and 2) the macropore system was mapped in detail. Each plot was subdivided into 0.5 m^2 raster elements. For each element, macropores that were connected to the soil surface were counted and their depth and diameter were measured using a vernier caliper and a wire. Table 2 gives the results of the macropore mapping at the two plots, i.e., the number of macropores per unit area, subdivided into four diameter classes, and their average length. Note that the averages and standard deviations in Table 2 were each obtained from 8 measurements, as each plot consisted of 8 raster elements. As the number and lengths of the macropores at the two plots match, again, within their standard deviations, we can safely assume that the macropore system at the irrigation plot can be statistically characterized by these values. In a next step, macroporous and non macroporous soil samples

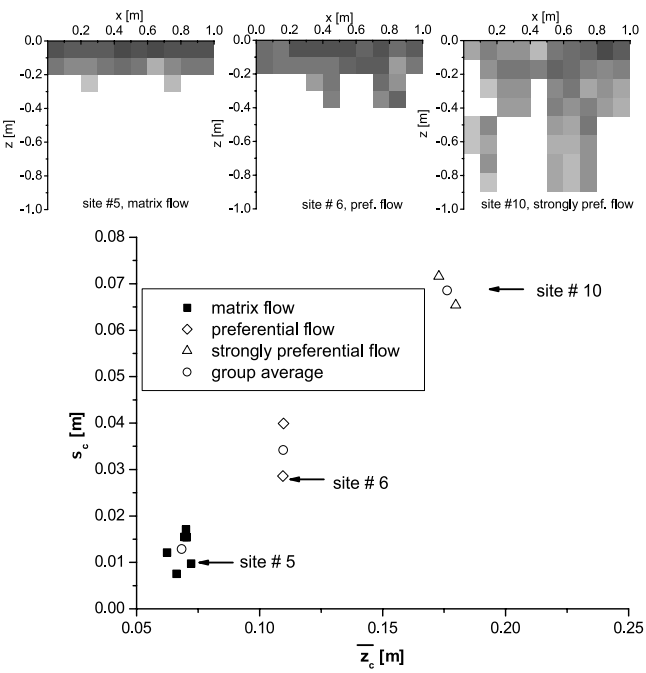

Figure 3. (bottom) Standard deviations σ_c plotted against the averages $\bar{z}_c$ of the observed vertical bromide transport distances at 10 tracer experimental sites (Figure 1), grouped into three flow regimes. In the preferential flow patterns, bromide has moved deeper into the soil (larger $\bar{z}_c$) than in the matrix flow patterns. (top) Bromide patterns of the soil profile at sites 5, 6, and 10 one day after start of irrigation. Dark colors represent large bromide concentrations, while white represents zero concentration.

Table 2. Average Number N_r and Average Depth l_r of Macropores Per Unit Area as Well as the Corresponding Standard Deviations Measured on Plots 1 and 2, Subdivided Into Four Diameter Classes

	2–4 mm Diameter		4–6 mm Diameter		6–8 mm Diameter		>8 mm Diameter	
	Plot 1	Plot 2	Plot 1	Plot 2	Plot 1	Plot 2	Plot 1	Plot 2
N_r	18.5 ± 5.2	21.3 ± 5.6	11.8 ± 4.5	12.5 ± 2.9	3.3 ± 1.2	3.3 ± 1.0	2.2 ± 0.41	2.0 ± 0.0
l_r, cm	49.6 ± 21.9	50.6 ± 17.5	59.2 ± 17.9	59.0 ± 9.3	67.5 ± 8.5	67.5 ± 8.5	80 ± 5.3	78.3 ± 5.4

were extracted from two depths (0.2 and 0.4 m) at plots 1 and 2 to measure their hydraulic properties in the laboratory. The first two moments of the saturated hydraulic conductivity and the porosity are given in Table 3. The averages and standard deviations in Table 3 were each obtained from 25 samples. Again, there is a good agreement between the corresponding moments at the two plots. Hence we assume that the hydraulic properties of the irrigation plot may be characterized by these moments.

3.3. Catchment-Scale Experiments and Macrostates

3.3.1. Outline of Measurement Network

[18] Figure 1 gives an overview of the observational network in the Weiherbach catchment. Rainfall input was measured at three rain gages and streamflow was monitored at two stream gages, all at a temporal resolution of 6 minutes. The gauged catchment areas are 0.32 and 3.6 km^2. For the catchment-scale simulations of rainfall-runoff events we focus on two mayor flood events (June 1994 and August 1995) at the lower gage only (see Table 4). Soil moisture was measured at up to 61 locations at weekly intervals using two-rod TDR equipment that integrates over the upper 15 cm of the soil. As the total area is 3.6 km^2, a number of 61 measurement points translates into an average spacing of 250 m [*Western and Blöschl*, 1999]. The soil hydraulic properties of typical Weiherbach soils were measured in the laboratory using undisturbed soil samples along transects at several hillslopes, up to 200 samples per slope (Table 5) [*Schäfer*, 1999]. A soil map was compiled from texture information that was available on a regular grid of 50 m spacing. The macropore system was mapped at 15 sites in the catchment in a similar way as described above for the plot-scale sites. The topography was represented by a digital elevation model of 12.5 m grid spacing. Further details on the measurement program are given by *Zehe et al.* [2001].

3.3.2. Measurement of Soil Moisture Macrostate and Soil Properties

[19] The macrostate of the initial soil moisture pattern for both rainfall events was characterized by the spatial average, variance and the variogram computed from the 61 point observations, as well as by the point observations to condition the spatial soil moisture distribution to the local observations. The estimated variogram parameters are given in Table 6. For both events, the nugget of the variogram is about 50% of the total soil moisture variance which means that there exists significant small scale variability that is not captured by the point observations [see, e.g., *Western et al.*, 2002]. The nugget is a measure of the information of the microstate that is not retained in the macrostate.

[20] As expected, the catchment-scale pattern of soil types turned out to be highly organized. The soil catena at a typical hillslope is Calcaric Regosol in the top and mid slope sector and Colluvisol in the valleys. The spatial patterns of the macropore characteristics observed in the Weiherbach catchment are closely related to the soil catena. The macroporosities tend to be small in the dry Calcaric Regosols located at the top and mid slope, and larger in the moist and drained Colluvisols located at the hill foot [*Zehe and Flühler*, 2001b]. The observations at the 15 sites were used to choose a deterministic pattern of macroporosity for the catchment-scale simulations (see section 4.3.1). The number of worm burrows connected to the soil surface turned out to vary throughout the year. The macropore system in the plow horizon is partly destroyed by plowing in spring and rebuilt by the earthworms in summer and early fall. Therefore the number of macropores connected to the soil surface appears to peak in late summer or early fall.

4. Model and Model Setup

4.1. Model Outline

[21] Monte Carlo simulations were performed using a physically based model known as CATFLOW [*Maurer*, 1997; *Zehe et al.*, 2001]. The model subdivides a catchment into a number of hillslopes and a drainage network. Each hillslope is discretized along the main slope line into a two-dimensional vertical grid using curvilinear orthogonal coordinates. Each model element, as defined by the grid, extends over the width of the hillslope. The widths of the elements vary from the top to the foot of the hillslope. For each hillslope, the model simulates the soil water dynamics and solute transport based on the Richards equation in the mixed form as well as a transport equation of the convection diffusion type. The equations are numerically solved using an implicit mass conservative "Picard iteration" [*Celia and*

Table 3. Average Saturated Hydraulic Conductivity k_s and Porosity θ_s as Well as the Corresponding Standard Deviations Measured on Plots 1 and 2

	k_s, m s^{-1}		θ_s	
Profile Depth, m	Plot 1	Plot 2	Plot 1	Plot 2
0.2	$(4.9 \pm 4.8) \times 10^{-06}$	$(3.9 \pm 4.1) \times 10^{-06}$	0.44 ± 0.04	0.45 ± 0.05
0.4	$(1.6 \pm 2.2) \times 10^{-06}$	$(1.1 \pm 1.7) \times 10^{-06}$	0.41 ± 0.03	0.40 ± 0.02

Table 4. Measured Characteristics of Flood Events: Precipitation Depth P, Average Precipitation Intensity I, Peak Discharge at the Catchment Outlet Q_{max}, Event Runoff Coefficient C, Average Initial Soil Moisture $\bar{\theta}$, Spatial Variance Var_θ, and Number of Available TDR Observations in Space N_{obs}[a]

Event	Date	P, mm	I, mm h^{-1}	Q_{max}, m^3 s^{-1}	C	$\bar{\theta}$	Var_θ	N_{obs}
1	27 June 1994	78.3	22	7.9	0.12	0.25	0.32	61
2	13 Aug. 1995	73.2	23	3.2	0.07	0.26	0.41	57

[a]Weiherbach lower gage, 3.6 km^2 catchment area.

Bouloutas, 1990] and a random walk (particle tracking) scheme. The simulation time step is dynamically adjusted to achieve an optimal change of the simulated soil moisture per time step which assures fast convergence of the Picard iteration. The hillslope module can simulate infiltration excess runoff, saturation excess runoff, lateral water flow in the subsurface and return flow. However, in the Weiherbach catchment only infiltration excess runoff contributes to storm runoff and lateral flow does not play a role at the event scale. What is important is the redistribution of near surface soil moisture in controlling infiltration and surface runoff. As the portion the portion of the tile drained area in the catchment is smaller than 0.5%, we did not account for tile drains in the simulation. Surface runoff is then routed on the hillslopes, fed into the channel network and routed to the catchment outlet based on the convection diffusion approximation to the one-dimensional Saint-Venant equation.

[22] For simulations of plot-scale flow and transport we used the hillslope module of CATFLOW and conceptualized the soil block as a horizontal hillslope. At the plot scale we are interested in simulating flow and transport in the near field when the transport distance is smaller than the characteristic heterogeneity of the soil. In this early stage of transport, a dispersion coefficient is not well defined [*Matheron and de Marsily*, 1980] and the tracer pattern is dominated by the variability of the flow field related to the main soil heterogeneity [*Roth and Hammel*, 1996]. We therefore do not account for a separate dispersion coefficient in the transport equation. Subscale diffusive mixing is only represented by the molecular diffusion coefficient of the solute of interest. At the catchment scale only flow simulations have been performed, so no dispersion coefficient is needed.

[23] As preferential flow and transport are important in the Weiherbach catchment, their representation is described in some detail below. Preferential flow and transport are represented by a simplified, effective approach similar to the 1-D approach of *Zurmühl and Durner* [1996]. However, while *Zurmühl and Durner* [1996] used a bimodal function to account for high unsaturated conductivities at high water saturation values, we use a threshold value S_0 for the relative saturation S, instead. If S at a macroporous grid point at the soil surface exceeds this threshold, the bulk hydraulic conductivity, k^B, at this point is assumed to increase linearly as follows:

$$k^B = k_S + k_S f_m \frac{S - S_0}{1 - S_0} \qquad \text{if } S \geq S_0$$
$$k^B = k_S \text{ otherwise} \tag{1}$$
$$S = \frac{\theta - \theta_r}{\theta_s - \theta_r}$$

where k_s is the saturated hydraulic conductivity of the soil matrix, θ_s and θ_r are saturated and residual soil moisture, respectively, and θ is the soil moisture. The macroporosity factor, f_m, is defined as the ratio of the water flow rate in the macropores, Q_m, in a model element of area A and the saturated water flow rate in the soil matrix. It is therefore a characteristic soil property reflecting the maximum influence of active preferential pathways on the soil water movement:

$$f_m(z) = \frac{Q_m}{Q_{matrix}} \tag{2}$$

where Q_{matrix} and Q_m are the water flow rates in the matrix and the macropores, respectively. At the plot scale, macropores of different sizes were generated, macropore flow rates were assigned to each macropore and then equation (2) was used to calculate f_m (see section 4.2.1). At the catchment scale, f_m was directly chosen as different values on the top and the foot of each hillslope, guided by macropore volume measurements (see section 4.3.1).

[24] In all scenarios we chose the threshold S_0 equal to 0.8, which corresponds to a soil moisture value of 0.32 in the Colluvisol (see Table 5 for values of θ_s and θ_r). This is a plausible value as it is on the order of the field capacity for the soils in the Weiherbach catchment. It is likely that for relative saturation values above this threshold, free gravity water is present in the coarse pores of the soil, and this free water may percolate into macropores and start preferential flow. This plausible value of S_0 was corroborated by simulations at a number of space-time scales in the Weiherbach catchment: Plot-scale bromide transport was simu-

Table 5. Laboratory Measurements of Average Hydraulic Properties for Typical Weiherbach Soils[a]

	k_s, m s^{-1}	θ_s, m^3 m^{-3}	θ_r, m^3 m^{-3}	α, m^{-1}	n
Calcaric Regosol	2.1×10^{-6}	0.44	0.06	0.40	2.06
Colluvium	5.0×10^{-6}	0.40	0.04	1.90	1.25

[a]Definition of parameters after *van Genuchten* [1980] and *Mualem* [1976].

Table 6. Statistical Characteristics of the Catchment-Scale Initial Soil Moisture θ Derived from the TDR Measurements[a]

Event	Date	$\bar{\theta}$, $m^3\ m^{-3}$	Var_θ	N_{obs}	Range, m	Nugget	Sill	R^2_{RES}	R^2_{TOP}
1	27 June 1994	0.25	0.32	61	500	0.16	0.16	0.22	0.23
2	13 Aug. 1995	0.26	0.41	57	700	0.24	0.17	0.24	0.11

[a]Characteristics: Average $\bar{\theta}$, variance Var_θ, number of measurements in space N_{obs}, range, nugget, sill of variogram, and portion of spatial soil moisture variance explained by different proxies (R^2_{RES} residual water content and R^2_{TOP} topographical index; see section 4.3.2).

lated at three sites of different macroporosity in good accordance with experimental findings of short-term tracer experiments (see sections 5.2.1 and 5.2.2). Simulations of tracer transport and water dynamics at an entire hillslope over a period of two years matched the corresponding observations of a long term tracer experiment at the hillslope-scale well [*Zehe et al.*, 2001]. Furthermore, the model performed well in a continuous simulation of the hydrologic cycle of the Weiherbach catchment over a period of 1.5 years [*Zehe et al.*, 2001]. We therefore believe that this threshold approach is suitable for the conditions in the Weiherbach catchment.

[25] Below we describe the model setup. At both scales, the model setup consists of the generation of the media and the generation of initial soil moisture. For the generation of the media we used a single realization only to define the small-scale detail. This is because the focus of this paper is on the uncertainty imposed by the initial conditions rather than on the uncertainty imposed by the model parameters. For the generation of initial soil moisture we generated an ensemble of realizations. Each realization represents one possible microstate that is consistent with the observed macrostate.

4.2. Plot-Scale Model Setup

4.2.1. Plot-Scale Media Generation

[26] CATFLOW is a two dimensional model and was used to simulate the tracer movement in the two dimensional (vertical) soil profile. To account for lateral heterogeneity we represented the $1 \times 1 \times 1.2\ m^3$ soil block by 10 two-dimensional cross sections (slabs) of 0.1 m thickness. Each of these two dimensional cross sections was represented by a finite difference grid of $0.05 \times 0.05\ m^2$ cell size. The size of each surface element hence is $0.05 \times 0.1\ m^2$. In the simulations, each of the slabs was irrigated with a hypothetical tracer solution. All the ten tracer patterns simulated by the model where then used to analyze infiltration response. The following boundary conditions were chosen: free drainage at the bottom, atmospheric pressure at the upper boundary, no flux boundary on the faces of the slabs.

[27] We put a lot of emphasis on generating a macroporous medium with a realistic structure as observed in the field. As pointed out by *Webb and Anderson* [1996] and *Western et al.* [2001], the generation of a macroporous medium based on purely random space functions will not capture the connectivity of preferential pathways. At our field site, preferential pathways were mainly vertical earthworm burrows of cylindrical cross sections, i.e., there was perfect connectivity in the vertical and almost no connectivity in the lateral directions. To capture these features we used a simple statistical approach for generating a system of earthworm burrows. The pattern of the macroporosity factor f_m in the model domain was determined by first statistically generating a macropore pattern in the model soil for each slab using the observed number of macropores, for each radius class (see Table 2). The fraction of the plot that was allowed to be covered by the total cross-sectional area of $\bar{N}_r$ macropores in each radius class was taken as the probability of occurrence of a macropore in this class p_r (equation (3) and Table 7). We assumed that the locations of the macropores at the soil surface are laterally uncorrelated but possess a perfect correlation in the vertical direction. Each surface element of a slab ($0.05 \times 0.1\ m^2$ in size) was subdivided into pixels of πr_m^2 in size, where r_m is the average radius of a macropore in a radius class, i.e., 1.5, 2.5, 3.5 and 4.5 mm. By generating a uniformly distributed random number $\xi \in [0, 1]$ the existence of a macropore of radius r_m was simulated for each pixel as follows:

$$\begin{aligned} &\xi \in [0, 1 - p_r] \rightarrow \text{pixel contains no macropore} \\ &\xi \in (1 - p_r, 1] \rightarrow \text{pixel contains a macropore of radius } r_m \\ &p_r = \frac{1}{\bar{N}_r \pi r_m^2} \end{aligned} \quad (3)$$

If a pixel contained a macropore, the macropore length was simulated by generating a normally distributed random number using the average and the standard deviations of the length of a macropore in a class (Table 7). After the generation of the macropore pattern the maximum possible water flow rate summed over all macropores beneath a surface element was computed as a function of depth. To this end we assumed the experimentally determined saturated water flow rate $Q_m(r_m)$ in a macropore of a given radius (Table 7) to be a characteristic constant, multiplied the number of macropores of a given radius by the corresponding $Q_m(r_m)$ value and summed these values over all radii. The pattern of the macroporosity factor, f_m, was then computed using equation (2). In our model, the

Table 7. Data for Computing the Macroporosity Factor[a]

	r_m, m			
	0.0015	0.0025	0.0035	0.0045
p_r	5.2×10^{-4}	9.2×10^{-4}	5.1×10^{-4}	5.5×10^{-4}
$\bar{l}_r$, m	0.49 ± 0.22	0.59 ± 0.18	0.67 ± 0.09	0.80 ± 0.05
$Q_m(r_m)$, $m^3\ s^{-1}$	4.6×10^{-8}	3.5×10^{-7}	1.4×10^{-6}	3.8×10^{-6}

[a]Probability (p_r) of occurrence of a macropore of radius r_m, average $\bar{l}_r$ and standard deviation of the macropore length, determined on the basis of the measurements given in Table 3. The saturated water flow rates Q_m in a macropore of radius r_m were measured using macroporous soil samples [*Zehe and Flühler*, 2001a].

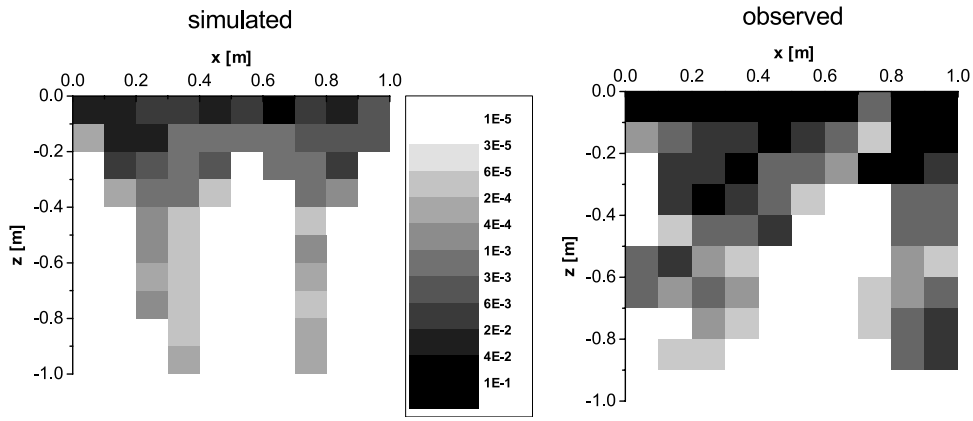

Figure 4. Simulated and observed preferential flow pattern (profiles of bromide concentrations) at one of the two profiles of site 10 one day after irrigation. For ease of comparison the simulated pattern was aggregated to the same grid of 10 × 10 cm as the observations. Units of concentration are [g kg^{-1}].

effective macropore system does not contribute to soil water movement for relative saturation values below S_0. If this threshold saturation at the soil surface is exceeded, the conductivity of the macroporous regions is increased (equation (1)) until it reaches a maximum value. For setting the matric hydraulic conductivity values the soil block was assumed to consist of two uniform horizons. From 0 to 30 cm depths and from 30 to 120 cm depths the matric hydraulic conductivities from Table 3 at 20 and 40 cm depths, respectively, were used, as the soil type did not vary at that scale.

4.2.2. Plot-Scale Generation of Initial Soil Moisture Microstates

[28] To account for the uncertainty of initial soil moisture we generated realizations of the field of initial soil moisture for each of the ten slabs using the turning band method [*Brooker*, 1985] assuming the initial soil moisture is normally distributed. All realizations had the same mean and variance as the observations (0.27 and 0.02 m^3 m^{-3}, respectively, see section 3.2.2). We chose a spherical variogram function and set the sill and the nugget of the variogram equal to the variance and the measurement error of the observed initial soil moisture, respectively. We distinguished two cases of statistical anisotropy. In the first case, the principal direction of anisotropy is horizontal. This represents a case where the field of initial soil moisture is dominated by the horizontal layering of the soil, so the range in horizontal direction was assumed as a_h = 1 m, which is equal to the width of the cross sections. The range in vertical direction was assumed as a_v = 0.15 m, which is equal to the length of the TDR rods. In the second case, the principal direction of anisotropy is vertical. This represents a case where the distribution of the initial soil moisture is dominated by vertical structures, e.g., as it may occur after a preferential flow event. The range in vertical direction was assumed as a_v = 0.55 m, reflecting the observed average depth of the macropores. The range in horizontal direction was assumed as a_h = 0.16 m, which is half the average distance between two macropores observed at the soil surface. The two cases will be referred to as horizontally and vertically structured. As the two cases cannot be distinguished using the above presented measurement strategy, they belong to the same observed macrostate. However, they differ in their microstates.

4.2.3. Plot-Scale Model Verification

[29] In order to test our approach of simulating preferential flow we generated macroporous media for sites 5, 6, and 10 in the Weiherbach catchment (see Figure 1) where different types of infiltration patterns were observed. The simulated and observed flow patterns were characterized by the average $\bar{z}_c$ and the variation σ_c of the vertical bromide transport distances z_c in the 5 × 10 × 120 cm^3 columns of the simulation soil block, and the average $\bar{z}_c$ and the variation σ_c of the vertical bromide transport distances z_c in the 10 × 10 × 100 cm^3 columns of the experiment at each of the three sites. As an example of the simulated bromide infiltration patterns, Figure 4 shows the results for site 10 along with the observations. The preferential structures of the simulations show qualitatively similar characteristics as those of the observed patterns. The statistics of the complete comparison of simulations and observations are given in Table 8. Table 8 shows that the average and standard deviation of the simulated bromide transport distances are both close to the observed values for all three plots. The results in Table 8 have been obtained by using detailed field data on the soil and macropore properties but without using the tracer measurements. Table 8 hence is a genuine test of the predictive performance of the model without any calibration. We therefore believe that our approach of simulating preferential flow as a threshold process and of generating macroporous media is a realistic representation of the conditions in the Weiherbach catchment.

4.3. Catchment-Scale Model Setup

4.3.1. Catchment-Scale Media Generation

[30] For the catchment-scale simulations, the Weiherbach catchment was subdivided into 169 hillslopes and an associated drainage channel network. The hillslope model elements, typically, are 5–20 m wide (depending on the position on the hillslope), 10 m long, and the depth of each element varies from 5 cm of the surface elements to 25 cm of the lower elements. The total soil depth represented by the model was 2 m. The Manning roughness coefficients for the hillslopes and the channels were taken from a number of

Table 8. Test of the Plot-Scale Model: Average z_c and Standard Deviation σ_c of the Bromide Transport Distance for the Simulated and Observed Flow Patterns[a]

Site	θ, $m^3\ m^{-3}$	Infiltration Type	Flow Pattern	$\bar{z}_c$, m	σ_c, m
10	0.27	preferential	observed	0.173 ± 0.025	0.071 ± 0.001
10	0.27	preferential	simulated	0.152 ± 0.019	0.058 ± 0.010
6	0.25	intermediate	observed	0.109 ± 0.006	0.040 ± 0.001
6	0.25	intermediate	simulated	0.098 ± 0.015	0.035 ± 0.008
5	0.23	matrix flow	observed	0.063 ± 0.003	0.013 ± 0.001
5	0.23	matrix flow	simulated	0.083 ± 0.027	0.048 ± 0.024

[a]In the case of the simulations, plus/minus values are the standard deviations of $\bar{z}_c$ and σ_c between realizations. In the case of the observations, plus/minus values have been calculated from the measurement errors by error propagation. θ [$m^3\ m^{-3}$] is the initial soil moisture. The corresponding observed flow patterns are given in Figures 2 and 3.

irrigation experiments performed in the catchment, as well as from the literature [see *Zehe et al.*, 2001]. For the hillslopes the following boundary conditions were chosen: free drainage at the bottom, mixed boundary conditions at the interface to the stream, atmospheric pressure at the upper boundary, no flux boundary at the watershed boundary. Because of the spatially highly organized hillslope soil catena observed in the Weiherbach catchment, all hillslopes in the model catchment were given the same relative catena with Calcaric Regosol in the upper 80% and Colluvisol in the lower 20% of the hill. The corresponding van Genuchten-Mualem parameters are listed in Table 5.

[31] The measurements of macroporosity at 15 sites in the Weiherbach catchment suggested high values in the moist Colluvisols at the hill foot and low values at the top and middle slope sectors (section 3.3.2). On the foot of the hillslopes the macropore volumes typically were 1.5×10^{-3} m^3 for 1 m^2 sampling area while on the top they typically were 0.6×10^{-3} m^3 [*Zehe*, 1999, Figure 4.1]. The most parsimonious approach that accounts for this structured variability is a deterministic pattern of the macroporosity factor with scaled values of the macroporosity factor at each hillslope. We chose the macroporosity factor to $0.6f_m$ at the upper 70% of the hillslope, $1.1f_m$ at the mid sector ranging from 70 to 85% of the hillslope, and $1.5f_m$ at the lowest 85 to 100% of the slope length, where f_m is the average macroporosity factor of the hillslopes. The depth of the macroporous layer was assumed to be constant throughout the whole catchment and was set to 0.5 m. The only remaining free parameter is the average macroporosity factor f_m of the hillslopes. As the number of macropores connected to the soil surface varies throughout the year, the f_m value has to be calibrated when we focus on the event scale. Within each model element we assumed that f_m represents all the subgrid variability of preferential flow in a lumped way, so we did not include the small-scale variations of bulk hydraulic conductivity due to individual macropores of the plot-scale set up.

4.3.2. Catchment-Scale Generation of Initial Soil Moisture Microstates

[32] To generate the initial soil moisture patterns at the catchment scale we used a combination of two-dimensional turning band simulations (TB) and simple updating (SUK). The TB algorithm [*Brooker*, 1985] was used to generate unconditional fields with the observed average, variance and range given in Table 6 assuming that soil moisture is normally distributed. To condition the TB generated fields to the soil moisture observations we resampled the field at the measurement locations and computed the differences (i.e., the residuals dθ) between observed and generated soil moisture. We interpolated the residuals using SUK and added them to the unconditional field, which produced a conditional field of initial soil moisture that gave exactly the observed soil moisture values at the measurement locations. SUK [*Bárdossy et al.*, 1996] is a geostatistical interpolation method that makes use of proxy information that is known at a higher spatial resolution than the variable of interest. It is based on a relationship between the variable of interest and a proxy variable (L) through a conditional mean m_L and variance Var_L. The soil moisture residual dθ at an arbitrary location is estimated as a sum of the Ordinary Kriging estimator and an estimator based on m_L plus a zero mean error ε_L with variance Var_L:

$$d\hat{\theta}(x) = \underbrace{\lambda_0\left(m_{L(x)} + \varepsilon_{L(x)}\right)}_{\text{proxy information}} + \underbrace{\sum_{i=1}^{N} \lambda_i d\theta(x_i)}_{\text{Kriging estimator (measurements)}} \quad (4)$$

For assisting in the interpolation on the catchment scale we examined two proxy variables. One proxy variable was the topographical index of *Beven and Kirkby* [1979], calculated from the digital elevation model at a 12.5 m resolution. The other proxy variable was the residual soil water content. It is defined here as the water content at a suction equal to the permanent wilting point, and is a measure of the amount of fine pores in the soil. It was estimated from the soil map at a 50 m resolution. For the two rainfall events, Table 6 lists the average, variance and range of the observed spatial distribution of measured soil moisture, as well as the coefficient of determination R^2 from a linear regression of soil moisture and the two proxies. The residual water content was the more consistent predictor of soil moisture for the two events although the coefficients of determination are small. We therefore used residual water content as a proxy variable in the interpolation of the soil moisture residuals to condition the TB generated fields. Within each model element we assumed that the soil moisture so estimated is a representative value over the entire element, so we did not include the small-scale variations of soil moisture of the plot-scale set up.

4.3.3. Catchment-Scale Model Calibration and Verification

[33] We calibrated the catchment-scale model by adjusting the macroporosity factor. We estimated the initial soil moisture patterns by interpolating the observations using SUK interpolation in a similar way as equation (4), but θ was interpolated rather than dθ. For rainfall event 1, which occurred in June 1994, we found an optimum macroporosity factor of $f_m = 2.1$. The simulated hydrographs for f_m values ranging from 0 to 3 are shown in Figure 5 (top) along with the calibration result. *Zehe et al.* [2001] used the same value of $f_m = 2.1$ in long term simulations of the complete hydrologic cycle of the Weiherbach catchment which produced unbiased runoff simulations. The rainfall events 1 (June 1994) and 2 (August 1995) are very similar in terms of their magnitudes, average intensities (Table 4) and initial soil moistures. However, the corresponding event runoff coefficients calculated from the observed hydrographs differ

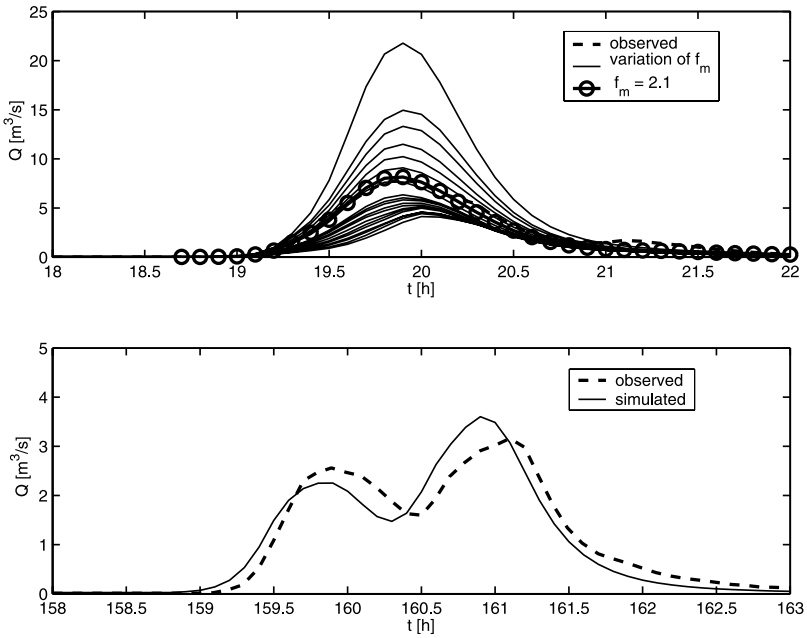

Figure 5. (top) Simulated discharges (thin solid lines) for event 1 (27 June 1994) for macroporosity factors ranging from $f_m = 0$ to 3. Increasing values of f_m correspond to decreasing runoff. The best fit to the observed hydrograph is obtained for $f_m = 2.1$ (circles). (bottom) Event 2 (13 August 1995) and best fit simulation with $f_m = 3.2$. Weiherbach catchment, 3.6 km^2 catchment area.

by a factor of almost 2 (Table 4). Apparently, the infiltration capacity of the soil was higher in August 1995 than it was in June 1994. This difference is likely related to a seasonal variation of the number of macropores (i.e., earthworm burrows) that are connected to the soil surface. This interpretation is consistent with the findings of several authors discussed in a review of *Flury* [1996, pp. 34–36] on transport of pesticides in the soil. Flury notes that continuous macropores are disrupted by plowing e.g., in spring and reconnected to the soil surface by earthworm activity during summer. For an accurate simulation of event 2 we had to increase the f_m value to 3.2 (Figure 5, bottom). As we allowed some degree of calibration for both events (Figure 5), the comparison cannot be considered a full verification. However, we only adjusted a single parameter (f_m) and the shape of the simulated hydrographs is very close to the observed hydrographs for both events. We therefore believe that the model is a realistic representation of the runoff processes in the Weiherbach catchment with the caveat that f_m is difficult to estimate a priori. As the focus of the further simulations was on event 2, we used an average f_m value of 3.2.

5. Monte Carlo Simulation Results

5.1. Simulated Plot-Scale Tracer Experiments

[34] For the plot-scale simulation study we generated three media of $1 \times 1 \times 1.2$ m^3 in size, one with a macroporosity factor as observed during the field experiment at site 10 (termed plot A), one with a macroporosity factor that was one tenth of the observed value at site 10 (termed plot B), and one without macroporosity ($f_m = 0$) (termed plot C). We varied the average initial soil moisture from 0.14 to 0.38 $m^3\ m^{-3}$ in steps of 0.01 $m^3\ m^{-3}$ to examine its effect on the predictability of hydrologic response. We assumed a standard deviation of 0.02 $m^3 m^{-3}$ which is the observed value (see section 3.2.2). For each of these cases we generated 40 realizations of soil moisture patterns by the Turning Band method. The irrigation depth and the bromide concentration in all simulations were set to $I_C = 25.3$ mm and $C = 0.165$ g L^{-1}, respectively, which are the same values as in the field experiment. The irrigation was simulated at 2 different average intensities, at 11 mm h^{-1} which is the same value as in the field experiment and at 2.2 mm h^{-1}. The irrigation was represented by constant intensity rainfall over 2.3 h and 11.5 h for the two average intensities to keep rainfall depth the same. As all the soil profiles in the field were excavated one day after the onset of irrigation, the simulation time was one day in all cases.

[35] To characterize each simulated tracer pattern we computed the average $\bar{z}_c$ and the standard deviation σ_c of the vertical bromide transport distances for the simulated pattern, as these parameters have been useful in identifying the presence of preferential flow in the observed patterns (compare Figure 3 and section 3.3). To characterize the ensemble of simulated tracer patterns, we calculated the coefficient of variation C_v and the scaled range n_s of the average bromide transport distance $\bar{z}_c^i$ within all $N_{trial} = 40$ trials (i.e., realizations) of a given average initial soil moisture:

$$\bar{\zeta}_c = \frac{1}{N_{trial}} \sum_{i=1}^{N_{trial}} \bar{z}_c^i, \quad \phi_c = \sqrt{\frac{1}{N_{trial}-1} \sum_{i=1}^{N_{trial}} \left(\bar{z}_c^i - \bar{\zeta}_c\right)^2}$$

$$C_v = \frac{\phi_c}{\bar{\zeta}_c}$$

$$n_s = \frac{\max\left(\bar{z}_c^i\right) - \min\left(\bar{z}_c^i\right)}{\bar{\zeta}_c} \tag{5}$$

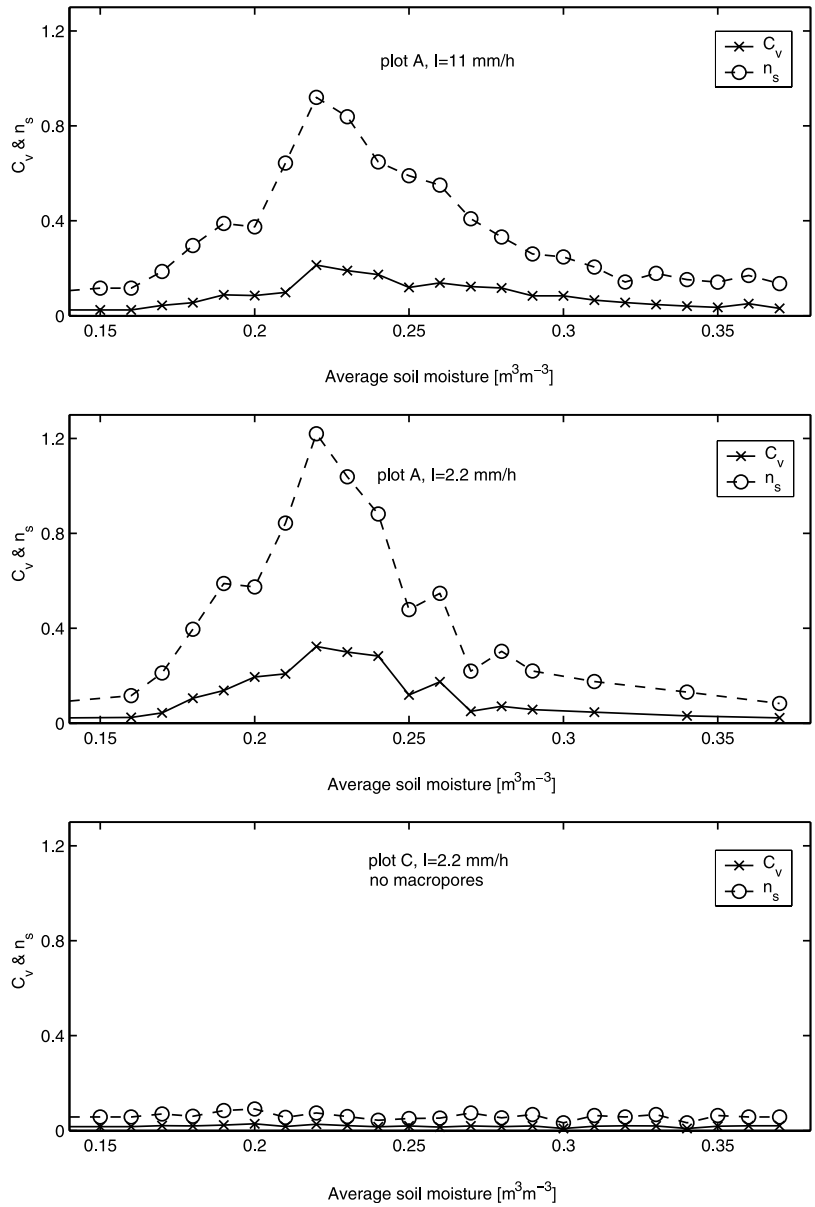

Figure 6. Coefficient of variation C_v and scaled range n_s of the average bromide transport distance $\bar{z}_c$ resulting from differences in the microstate of initial soil moisture plotted against the average initial soil moisture $\bar{\theta}$. Simulations at hypothetical plot A for irrigation rates of (top) 11 mm h^{-1} and (middle) 2.2 mm h^{-1}. (bottom) C_v and n_s of hypothetical plot C (without macropores). The threshold saturation S_0 for initiation of macropore flow corresponds to a soil moisture value of 0.32 m^3 m^{-3}.

C_v and n_s are used to quantify the effect of uncertain initial soil moisture on the infiltration response.

5.1.1. Simulations With Observed Macroporosity and I = 11 mm h^{-1}

[36] Figure 6 (top) shows the coefficient of variation C_v and the scaled range n_s of the average bromide transport distance $\bar{z}_c$ within all trials plotted against the average initial soil moisture $\bar{\theta}$ for the simulated irrigation at the high irrigation rate of I = 11 mm h^{-1}. For initial soil moistures below about 0.19 m^3 m^{-3} and above about 0.28 m^3 m^{-3} the coefficient of variation C_v and the scaled range n_s are relatively small. This means that the repeated trials of the simulated irrigation lead to the same type of infiltration, low average bromide transport distances $\bar{z}_c$ for average initial moisture values $\bar{\theta}$ below 0.19 m^3 m^{-3}, and large $\bar{z}_c$ values for $\bar{\theta}$ exceeding 0.28 m^3 m^{-3}. The uncertainty of the initial soil moisture pattern expressed as the different possible initial microstates hence does not significantly affect the type of simulated flow pattern. For average initial soil moistures ranging from 0.19 to 0.28 m^3 m^{-3} the simulations produce a completely different behavior. In this range, the uncertainty of the initial state is amplified, leading to a coefficient of variation of up to 0.21 and a scaled range of up to 0.9. Thus, depending on the microstate of the initial soil moisture patterns, either fast or slow transport can establish during the infiltration event, which is reflected by a large variation of the bromide transport distances between the trials. We call this range of average initial soil

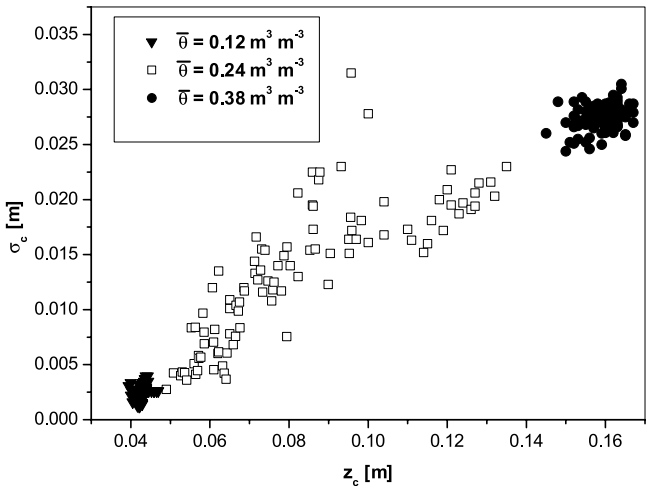

Figure 7. Standard deviations σ_c plotted against the averages $\bar{z}_c$ of the simulated vertical bromide transport distances for average initial soil moisture values of 0.14, 0.24, and 0.38 $m^3\ m^{-3}$. The bromide centers of mass of the flow patterns in the unstable range ($\bar{\theta} = 0.24$) cover nearly the whole spectrum of infiltration regimes from matrix flow dominated to strongly preferential patterns. The irrigation depth and rate were 25.3 mm and 2.2 mm h^{-1}, respectively (hypothetical plot B).

moisture the unstable range because different microstates that belong to the same observed macrostate of initial soil moisture can lead either to attenuated or to enhanced infiltration relative to the average conditions.

5.1.2. Simulations With Observed Macroporosity and Smaller I

[37] Figure 6 (middle) shows the coefficient of variation and the scaled range of $\bar{z}_c$ within all trials plotted against the average initial soil moisture $\bar{\theta}$ for the simulated irrigation of plot A at a low irrigation intensity of I = 2.2 mm h^{-1}. The results are similar to the previous case but the coefficient of variation and the scaled range in the unstable range of initial soil moisture (0.19 to 0.28 $m^3\ m^{-3}$) increase to values of 0.35 and 1.2, respectively. This means that reducing the intensity enhances the dependence of the simulated flow patterns on the microstate of the initial soil moisture. The minimum average bromide transport distance calculated in the repeated trials for an average initial soil moisture of 0.22 $m^3\ m^{-3}$ is only one third of the maximum value. This wide spreading of the average bromide transport distances indicates that the expected type of infiltration can be fast, slow or a combination thereof. For average initial soil moisture values below 0.19 $m^3\ m^{-3}$ and above 0.28 $m^3\ m^{-3}$ the infiltration type is stable and repeated trials lead to a low variation of the average bromide transport distance.

[38] To examine the flow regime of the tracer patterns resulting from the repeated trials at 0.14, 0.24 and 0.38 $m^3\ m^{-3}$ average soil moisture in more detail, the average bromide transport distance $\bar{z}_c$ has been plotted against the variation of the bromide transport distance σ_c in Figure 7. To interpret the flow regime in Figure 7, the observations in Figure 3 can be recalled which suggest that low values of $\bar{z}_c$ and σ_c are associated with matrix flow while large values of $\bar{z}_c$ and σ_c are associated with preferential flow. This means that for the small average moisture values ($\bar{\theta} = 0.14\ m^3\ m^{-3}$) in Figure 7 matrix flow occurred alone while for the large average moisture values ($\bar{\theta} = 0.38\ m^3\ m^{-3}$) preferential flow occurred in all cases. In contrast, the parameters associated with $\bar{\theta} = 0.24\ m^3\ m^{-3}$ (circles in Figure 7) cover nearly the whole range between the two extreme ends of the spectrum of infiltration regimes. If we adopt the classification of flow patterns into matrix flow dominated, intermediate, preferential and strongly preferential for $\bar{z}_c$ values ranging from 0.04–0.07, 0.07–0.10, 0.10–0.13 and 0.13–0.17 m from Figure 3 to the simulations, we obtain the following results: For an average initial soil moisture of 0.24 $m^3\ m^{-3}$, the simulated repetition of the tracer experiment leads to matrix flow patterns in 39%, intermediate flow patterns in 38%, preferential flow patterns in 20% and strongly preferential flow patterns in 2% of the trials. Any type of flow pattern seems to be possible with a finite probability, so the observed macrostate of initial soil moisture may not be related to a unique type of flow regime. In the stable ranges, the knowledge of the macrostate of initial soil moisture is sufficient to predict the type of flow pattern. In the unstable range, however, this is not the case.

[39] Table 9 gives the maximum and minimum values of average bromide transport distance $\bar{z}_c$ at the average initial soil moisture value of maximum uncertainty as well as the spatial correlation between the corresponding realization of the initial soil moisture pattern and the bulk hydraulic conductivity k^B of the model soil. Table 9 indicates that positive correlations between local saturation and local macropore-related hydraulic conductivity produce large average transport distances, while negative correlations produce much smaller transport distances. The correlation coefficients are only of the order ±0.3, which are weak correlations. This means that at the moisture state where the uncertainties in the microstate translate into the largest uncertainties in hydrologic response, small differences in the hydrologic conditions can lead to drastic differences in hydrologic response. As can be seen from Table 9, the principal direction of anisotropy of the generated initial soil moisture has only a small influence on the state-dependent uncertainty of the simulated tracer patterns.

5.1.3. Simulations With Reduced Macroporosity

[40] For comparison, we reduced the macroporosity factor to one tenth of the observed value and reran the simulations. Interestingly, this case produced qualitatively very similar results to the previous cases. Uncertain initial conditions, again, produced highly uncertain infiltration patterns in the unstable range of average moisture between about 0.19 and 0.28 $m^3\ m^{-3}$. In the stable range, i.e., for values either smaller than 0.19 or larger than 0.28 $m^3\ m^{-3}$, the type of the simulated infiltration patterns was stable. However, if the macroporosity factor of the model soil is reduced to zero (Figure 6, bottom) both the coefficient of variation and the scaled range get very small. This means that, no matter what the initial soil moisture pattern is, the resulting infiltration pattern will always look similar. The state-dependent predictability of the simulated plot-scale tracer pattern is therefore a direct consequence of the macroporous heterogeneity and the presence of a threshold process.

5.2. Simulated Catchment Response

[41] To quantify the impact of uncertain initial soil moisture on flood response at the catchment scale we

Table 9. Minima and Maxima of the Average Bromide Transport Distance $\bar{z}_c$, Average Initial Soil Moisture $\bar{\theta}$, and Correlation Coefficient R Between the Initial Soil Moisture Pattern and the Bulk Hydraulic Conductivity k^B for Each Case of Anisotropy for Simulation Results

	$\bar{z}_c$, m	R	$\bar{\theta}$, $m^3\ m^{-3}$	Anisotropy Case
		Plot A		
Minima	0.049	−0.31	0.22	horizontal
Maxima	0.135	0.24	0.22	horizontal
Minima	0.056	−0.28	0.22	vertical
Maxima	0.122	0.26	0.22	vertical
		Plot B		
Minima	0.046	−0.39	0.22	horizontal
Maxima	0.122	0.28	0.22	horizontal
Minima	0.060	−0.14	0.22	vertical
Maxima	0.107	0.21	0.22	vertical

simulated the runoff response to rainfall event 2 using 20 turning band generated fields of initial soil moisture conditioned to the soil moisture observations prior to event 2. The sill, nugget and range of the generated initial soil moisture patterns were those in Table 6 (event 2). The spatial mean of all of these fields was 0.26 $m^3\ m^{-3}$ consistent with the observed soil moisture at the beginning of this event (Table 4). We then added constant values ranging from -0.12 to 0.12 $m^3\ m^{-3}$ to each realization in order to obtain fields with average initial soil moisture ranging from 0.14 $m^3\ m^{-3}$ to 0.38 $m^3\ m^{-3}$ in steps of 0.02 $m^3\ m^{-3}$, similar to the plot-scale analysis. The different realizations of the initial soil moisture pattern represent, again, different possible microstates consistent with the observed macrostate of initial soil moisture. To investigate the influence of rainfall intensity we repeated the Monte Carlo simulations of flood response using a hypothetical rainfall event for which we reduced the intensity to 50% and scaled time to 200%, thus retaining the total rainfall depth. We term this event the reduced event 2.

5.2.1. Monte Carlo Simulations of Event 2

[42] To characterize the ensemble of simulated flood hydrographs, we calculated the coefficient of variation C_v and the scaled range n_s of the flood peaks Q_{max} within all 20 trials of a given average initial soil moisture in an analogous way to equation (5). Figure 8 (top) shows the coefficient of variation C_v and the scaled range n_s of Q_{max} plotted versus average initial soil moisture. For initial soil moistures below about 0.18 $m^3\ m^{-3}$ and above about 0.30 $m^3\ m^{-3}$ the coefficient of variation C_v and the scaled range n_s are relatively small. This means that the repeated trials of the simulated rainfall events lead to consistent runoff response, small flood peaks for average initial moisture values $\bar{\theta}$ below 0.18 $m^3\ m^{-3}$, and large flood peaks for $\bar{\theta}$ exceeding 0.30 $m^3\ m^{-3}$. The uncertainty of the initial soil moisture pattern expressed as the different possible initial microstates hence does not significantly affect flood response for these conditions. For average initial soil moistures ranging from about 0.18 to 0.30 $m^3\ m^{-3}$, however, the uncertainty of the initial state is amplified, leading to a coefficient of variation of up to 0.08 and a scaled range of up to 0.32. Thus, for the same observed macrostate of initial soil moisture the flood peaks can differ remarkably, depending on the microstate.

[43] The shape of the dependence of the coefficient of variation C_v and the scaled range n_s on the average initial soil moisture in Figure 8 (top) is similar to the corresponding values for the plot scale in Figure 6 (top and middle). The soil moisture associated with the maximum uncertainty is 0.24 $m^3\ m^{-3}$ which is close to a value of 0.22 $m^3\ m^{-3}$ found at the plot scale. However, the scaled range and coefficient of variation computed for Q_{max} are

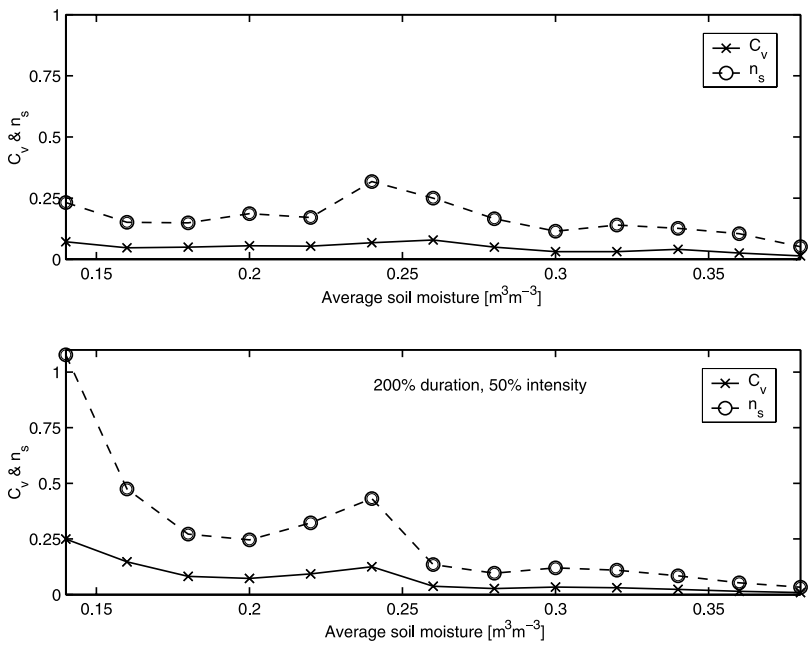

Figure 8. Coefficient of variation C_v and scaled range n_s of flood peaks resulting from differences in the microstate of initial soil moisture plotted against the average initial soil moisture $\bar{\theta}$. Simulations for the Weiherbach catchment (3.6 km^2). (top) Original event 2; (bottom) reduced event 2.

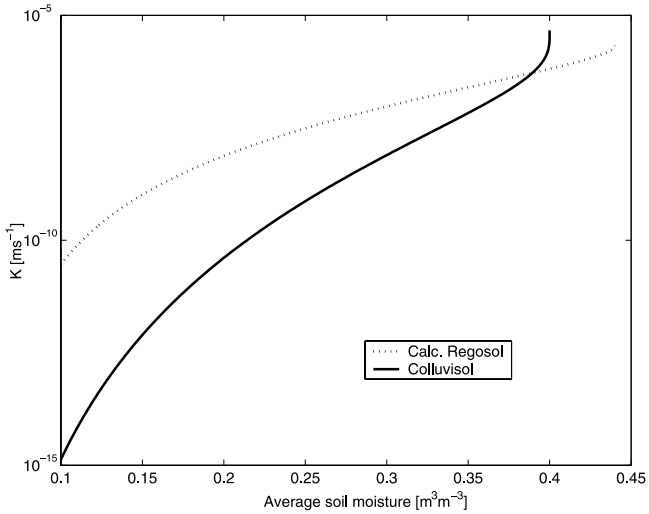

Figure 9. Characteristic unsaturated hydraulic conductivity curves for the Calcaric Regosol (dashed) and the Colluvisol (solid). K is the unsaturated hydraulic conductivity, and θ is the soil moisture.

clearly smaller than the corresponding values computed for the average bromide transport distance $\bar{z}_c$. In contrast to the plot scale, the effect of uncertain initial soil moisture on the flood peaks increases as the average initial soil moisture approaches very small values. This increase is related to the presence of two soil types in the case of the catchment scale. As can be seen from Figure 9, over most of the soil moisture range, the unsaturated hydraulic conductivity of the Calcaric Regosol is larger than that of the Colluvisol. In the dry case, infiltration only occurs through matrix flow which will be different in these two soils. The superposition of different microstates of the initial soil moisture pattern on the soil type related conductivity pattern will therefore produce large differences in infiltration and hence runoff generation.

[44] To further highlight the dependence of the simulated hydrographs on the microstate of initial soil moisture Figure 10 shows the simulated catchment response for average initial soil moisture values of 0.14 m^3 m^{-3}, 0.24 m^3 m^{-3} and 0.38 m^3 m^{-3}. In the dry case (Figure 10, top left), the runoff response to the first rainfall burst is remarkably large and there is almost no response to the second burst 2. This counterintuitive result is due to the soil moisture being below the threshold for the initiation of macropore flow, so no macropore flow takes place at the beginning of the event. The matrix initial soil hydraulic conductivity associated with the dry soils is also very low (10^{-13}–10^{-9} m s^{-1}). This conductivity corresponds to a rainfall intensity of less than 0.004 mm h^{-1}, which is much lower than the average precipitation intensity of 22 mm h^{-1} (Table 4), so most of the rainfall becomes runoff at the beginning of the first peak. During the second part of the event, however, the soil wets up and water may infiltrate and not produce runoff. The runoff response in the wet case (Figure 10, bottom right) is quite different with moderate response to the first rain burst and large response to the second burst. Because of the high initial relative saturation (S = 0.95 in the Colluvisol and 0.86 in the Calcaric Regosol) the initial hydraulic conductivity of the soil is on the order of 10^{-5} m s^{-1} (including macropore effects). This value corresponds to a rainfall intensity of 36 mm h^{-1} and exceeds the average rainfall intensity of 22 mm h^{-1}, so the first flood peak in the wet case is smaller than that in the dry case. The runoff response in the intermediate case (Figure 10, bottom left) is lower than in the two extreme cases. This is because,

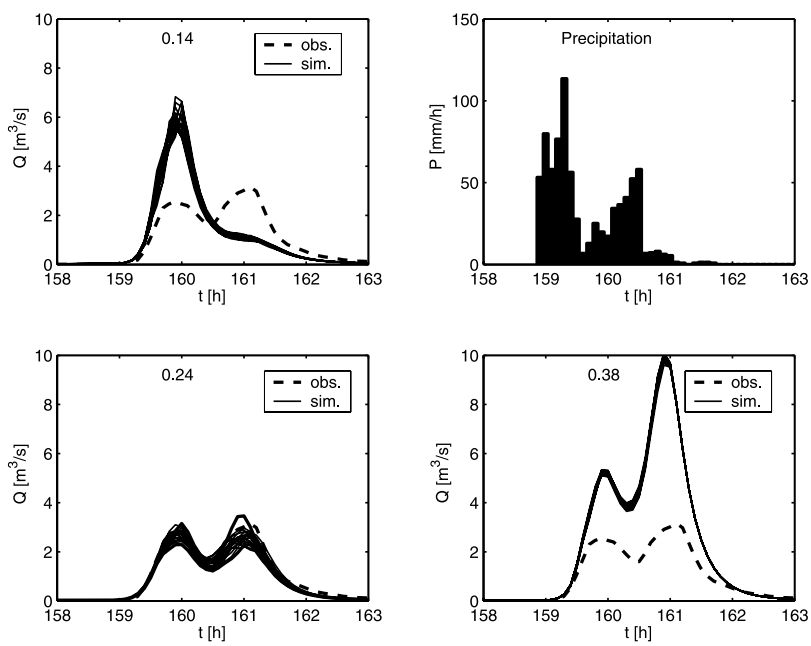

Figure 10. Simulated catchment runoff response (thin lines) to rainfall event 2 for average initial soil moisture values of (top left) 0.14, (bottom left) 0.24, and (bottom right) 0.38. The thick lines in the bottom left panel represent the largest and smallest simulated flood response in the ensemble of realizations. The dashed lines are the observed hydrographs. (top right) Hyetograph of event 2. Weiherbach catchment, 3.6 km^2 catchment area.

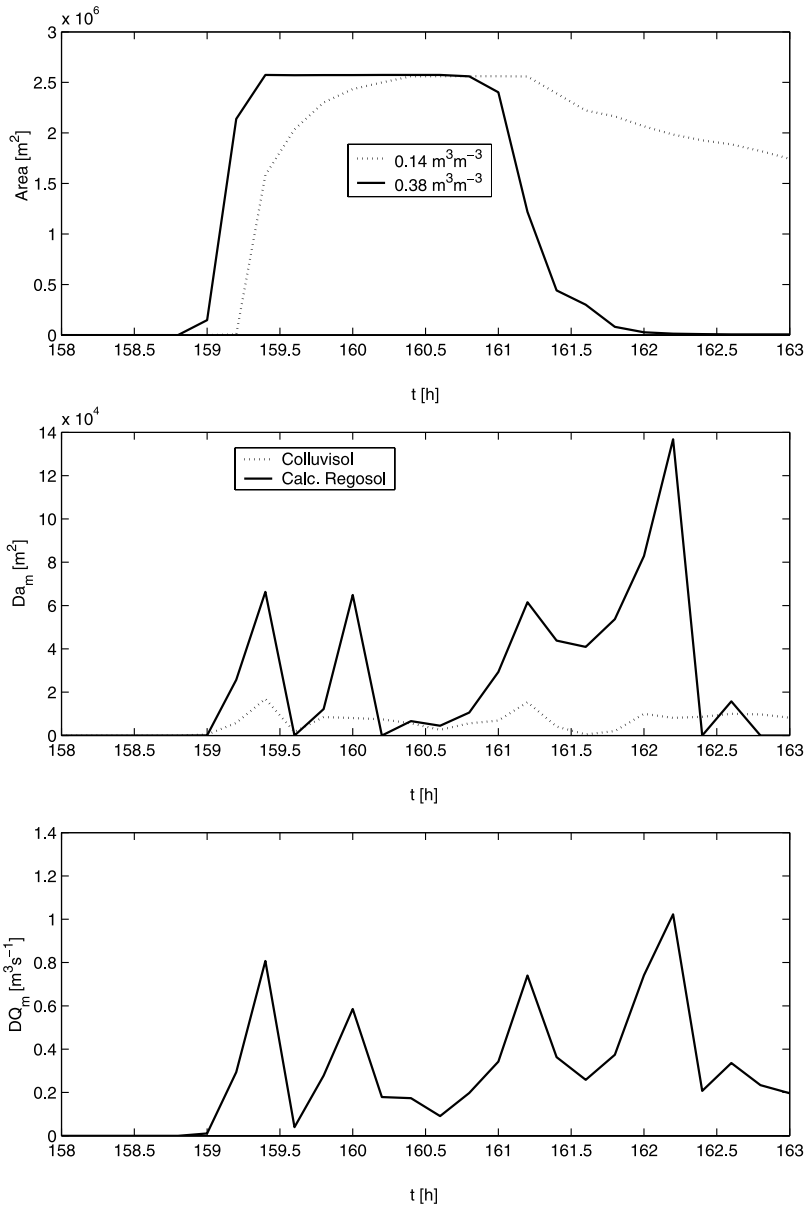

Figure 11. (top) Saturated areas a_{ss} for simulated catchment response to rainfall event 2 at an average initial soil moisture of 0.38 m^3 m^{-3} (solid line) and 0.14 m^3 m^{-3} (dotted line). (middle) Difference Δa_m (Da_m)of the area where S exceeds 0.9 for the smallest and largest simulated flood response to event 2 at an average initial soil moisture of 0.24 m^3 m^{-3}, separately for the two soils. Δa_m is a measure of the difference in the contribution of preferential flow. (bottom) Difference in infiltration capacity ΔQ_m (DQ_m)caused by the difference in areas exhibiting preferential flow (equation (7)). Weiherbach catchment, 3.6 km^2 catchment area.

in this case, the hydraulic conductivity is large enough for a large part of rainfall to infiltrate, and the soil is dry enough to store water and not produce saturation excess runoff.

[45] The hydrographs for low average initial moisture show some dependence on the microstate of the initial soil moisture patterns, those for the high average initial moisture show almost no dependence (Figure 10). In contrast, the simulated hydrographs for the intermediate average initial soil moisture of 0.24 m^3 m^{-3} exhibit a significant dependence on the soil moisture microstate. The difference between the two enveloping hydrographs is on the order of 1 m^3 s^{-1} over more than an hour (t = 160–161 h) which is large as compared to an observed peak of less than 3 m^3 s^{-1}. These results are consistent with the peak in sensitivity of n_s = 0.32 in Figure 8.

[46] To better understand the differences in the runoff responses in the dry and wet cases, we computed the saturated area a_{ss} as the total area where the surface grid elements were saturated (i.e., relative saturation S = 1). This corresponds to the upper 5 cm of the soil, so this definition of saturation does not necessarily imply that the entire 2 m soil profile is saturated. The relative saturation S of the upper layer controls whether macropores start to contribute to infiltration or not (equation (1)). Figure 11 (top) shows

the time series of a_{ss} for the dry and wet cases of Figure 10. In the dry case, a_{ss} increases less steep and at a later time than in the wet case, but toward the end of the event it remains at a larger value for a longer time. This is because the soils are not as readily drained as in the wet case since the lower layers are drier. We now intend to explain the difference between the two enveloping hydrographs simulated for the intermediate average soil moisture conditions (i.e., thick lines in Figure 10, bottom left). For the lower and upper enveloping hydrographs the total areas where soil water saturation in the upper 5 cm exceeded a value of 0.9 were computed and denoted as a_m^l and a_m^u, respectively. In each case, this is the total area in the catchment where strong preferential flow may take place according to equation (1). We then calculated the difference of these two areas:

$$a_m(t) \equiv \{a|S > 0.9\}$$
$$\Delta a_m(t) = a_m^l - a_m^u \tag{6}$$

This was done for each soil type separately. The results are the Δa_m curves shown in the Figure 11 (middle). These curves represent the difference in the total area where preferential flow takes place. As expected, the differences are always positive which means that the total area where preferential flow takes place is always larger for the lower flood envelope than for the upper flood envelope. Because of the larger area where preferential flow is initiated, more water can infiltrate. To obtain a quantitative estimate of the difference between the infiltrating water in the two cases we multiplied Δa_m by the hydraulic conductivity and the corresponding macroporosity factors (see definition in equation (1)).

$$\Delta Q_m(t) = \Delta a_m(t) k(\theta) f_m \frac{S - S_0}{1 - S_0} \tag{7}$$

This was done for each soil type separately. The sum of the resulting ΔQ_m values of the two soils is shown in Figure 11 (bottom). Figure 11 (middle) indicates that the difference of the total infiltrating water is on the order of 1 $m^3 s^{-1}$, which is consistent with the difference of the two enveloping hydrographs in Figure 10 (bottom left). This corroborates our interpretation that the differences in the simulated flood responses stem from the differences in the total areas that exhibit preferential flow in the catchment.

5.2.2. Simulations With Reduced Precipitation Intensity

[47] For the case of reduced precipitation intensities (reduced event 2) Figure 8 (bottom) shows the coefficient of variation C_v and the scaled range n_s of the flood peaks Q_{max} that result from the uncertainties in the microstate of soil moisture, plotted versus average initial soil moisture. The simulations yield similar result as the corresponding simulations of the original rainfall event 2 (Figure 8, top) but the uncertainty increases. For the intermediate average initial soil moisture range the coefficient of variation and the scaled range give maxima of about 0.15 and 0.42, respectively. In contrast to the original event 2, the dependence on the microstate of the initial soil moisture increases strongly as soil moisture approaches dry conditions and the maximum coefficient of variation and the scaled range for dry soils are 0.25 and 1.1, respectively. It appears that, as the rainfall forcing decreases in intensity, the role of the nonlinearity increases. At the dry end of soil moisture the uncertainty is particularly high. This again, is related to contrasting soil hydraulic characteristics of the two soils in the catchment (see Figure 9).

6. Discussion and Conclusions

6.1. State Dependence of Predictability

[48] We have examined the effect of uncertainty in the microstate of initial soil moisture on the predictability of hydrologic response at the plot and catchment scales. The Monte Carlo analyses indicate that considerable uncertainty does exist at both scales, so the predictability is indeed limited by the availability of only a finite number of measurements to specify the macrostates of initial soil moisture. This is consistent with the qualitative assessment of *Grayson et al.* [1995] and *Merz and Bárdossy* [1998] and others that different spatial patterns of initial soil moisture can produce vastly different results of runoff response even if the spatial statistical distributions are the same. At the plot scale, the processes may switch between matrix and preferential flow, and at the catchment-scale processes may switch between runoff generation mechanisms and these transitions, under some conditions, cannot be captured by the measurements. The uncertainty in hydrologic response, again depending on the conditions and the variable examined, may range up to a coefficient of variation of 0.4 and a scaled range of the uncertainty of 1 implying a maximum absolute error of 100%.

[49] The simulations indicate that the predictability of the hydrologic response depends on the average initial state of soil moisture. At both the plot and catchment scales there exists an unstable range where the predictability of hydrologic response is poor, and a stable range where the predictability is significantly better. The unstable range ranges from an average soil moisture of about 0.18 to 0.30 $m^3 m^{-3}$ at both scales and the uncertainty peaks around 0.22 m^3 m^{-3} (Figure 6, top, and Figure 8, top). For dry conditions (average initial soil moisture below 0.18 m^3 m^{-3}) and for wet conditions (average initial soil moisture above 0.30 m^3 m^{-3}) the predictability is much better, so this is the stable range. Clearly, this state-dependent predictability is related to the presence of threshold processes. If the system is close to the threshold the predictability is poor. The main threshold in the Weiherbach catchment is the transition from matrix to macropore flow. We conceptualized this transition by a threshold value of relative saturation for the initiation of macropore flow which we set to $S_0 = 0.8$. This value is equivalent to a soil moisture of about 0.32 for the Weiherbach soils. The unstable range is below this threshold and this is because the initiation of macropore flow relevant to hydrologic response occurs during the event when the soil moisture has increased beyond that of the initial conditions. For different event rainfall depths the location of the unstable range will likely change from that in the simulations of this event. Also, in different environments with different soils the threshold value will be different from that in the Weiherbach catchment. It is important to note that storm runoff generation in the Weiherbach is by infiltration excess and there are essentially no subsurface lateral flows. In other catchments, saturation excess and/or subsurface storm flow may be the more important contributions to

storm runoff. Although the detailed characteristics will be different there is evidence that saturation excess runoff, for example, operates as a threshold process [e.g., *Western and Grayson*, 1998]. As the type of nonlinear behavior of a threshold process occurs in many environments and in many different processes one would expect this state-dependent predictability, albeit at different soil moisture states, to occur more universally.

[50] Representing the macrostate of initial soil moisture by the distribution function rather than by spatial patterns does not account for the small-scale details of the microstate. One of the important pieces of information that is lost is the correlation between local saturation and local macropore-related hydraulic conductivity. At the plot scale, if the soil was prone to switch from matrix to macropore flow, soil moisture microstates that were positively correlated with the bulk hydraulic conductivity yielded fast infiltration and transport associated with preferential flow. This positive correlation of some of the microstates stems from the superposition of the soil moisture microstates on the time invariant pattern of macroporosity. Other microstates exhibited negative correlations and these produced slow infiltration and transport associated with matrix flow (Table 9). The correlation becomes important because of the nonlinearity introduced by the threshold process. For a linear system one would expect the effects of the correlations to average out to a large degree. It was not possible to obtain estimates of this correlation from the field data as the soil moisture measurements and the mapping of the macropore system had to be done at separate plots because of the disturbance of the soil by each of these measurements. It is therefore not possible to include them in the description of the macrostate. Experimental findings of *Villholth et al.* [1998] and *Zehe and Flühler* [2001b] suggest that high values of initial saturation in macroporous subregions favor the occurrence of macropore flow, so positive correlations probably occur quite frequently. A similar effect occurs at the catchment scale. If the soil is prone to switch from matrix to macropore flow, microstates where, locally, soil moisture is large at a location of large macroporosities will produce much larger infiltration rates than if low soil moisture is colocated with large macroporosities. The time invariant patterns of macroporosity are associated with the hillslope soil catena and there is also the effect of the patterns of matric conductivity associated with different soil types. Figure 11 suggests that the uncertainty in flood response for the intermediate, unstable, initial soil moisture conditions is mainly due to differences in the total areas that exhibit preferential flow between different microstates.

6.2. Other Factors Controlling Predictability

[51] There are a number of other factors, in addition to the average initial moisture state, that control the effect of uncertainty in the microstate of initial soil moisture on the predictability of hydrologic response. The factors examined in this paper include rainfall intensity, macroporosity and scale.

[52] If we reduce the irrigation intensity at the plot scale from 11 to 2.2 mm h^{-1} the coefficient of variation between the realizations increases from 0.21 to 0.35 and the scaled range increases from 0.9 to 1.2 (Figure 6). If we reduce the average rainfall intensity at the catchment scale from 23 mm h^{-1} to 11.5 mm h^{-1} the coefficient of variation increases from 0.08 to 0.25 and the scaled range increases from 0.32 to 1.1 (Figure 8). This means that the predictability decreases with decreasing rainfall intensity at both scales. It appears that, as the rainfall forcing decreases in intensity, the role of the nonlinearity increases. This is because lower rainfall intensities are closer to a threshold where surface runoff may or may not be generated while large rainfall intensities will always produce surface runoff. It should be noted that the measure for predictability used here is a relative measure, i.e., the short bromide travel distances and the small flood peaks associated with the small intensities are relatively more uncertain than larger distances and larger flood peaks. When reducing rainfall intensities there is also a shift of the unstable range toward lower average initial soil moistures at the plot scale, and an additional unstable range emerges at low average initial soil moistures at the catchment scale. This, again, is related to the larger sensitivity of runoff response to uncertain initial conditions when rainfall intensity decreases. In the case of the catchment scale, the spatial pattern in matric hydraulic conductivities related to different soils types appears to produce this additional sensitivity at the dry end of initial conditions.

[53] It is interesting that the value of the macroporosity does not change the predictability. Plot-scale simulations performed with macroporosities of one tenth of the observed value produced very similar predictabilities as those with the observed values. This is because the main uncertainty is introduced by the transition between matrix and macropore flow rather than by the flow rate once the macropores have been activated. This is a reflection of the importance of the nonlinearity. However, if only matrix flow is allowed the uncertainty decreases vastly. A hydrologic system with only matrix flow is much more predictable than a system where a transition between matrix and macropore flow may take place.

[54] As simulations at the $1m^2$ plot scale and the 3.6 km^2 catchment scale have been performed in this paper we can draw conclusions on the scale dependence of predictability. The response at the plot scale is measured by an analysis of the vertical bromide transport distances of hypothetical irrigation experiments and the response at the catchment scale is measured by an analysis of the flood peak discharge of hypothetical rainfall events, so they are not strictly comparable. However, because of the similarity of flow and transport scales of motion we believe that general remarks on the relative orders of magnitude of the predictabilities are in place. As we go up in scale in the standard cases examined here, the coefficient of variation between the realizations decreases from 0.21 to 0.08 and the scaled range decreases from 0.9 to 0.32 (Figure 6, top, and Figure 8, top). This means that the predictability increases with scale with maximum absolute errors of 90% and 32% at the plot scale and the catchment scale, respectively. There are a number of considerations in interpreting this scale dependence. As one goes up in scale one would at least part of the variability expect to average out [see, e.g., *Blöschl*, 1999]. In the catchment-scale model, subgrid variability has been dealt with in a lumped way. Unlike at the plot scale where small-scale heterogeneities resulting from individual macropores were represented in the model, only a single effective value of the macroporosity factor f_m has been used

in each element of the catchment model. Because of this, one would not expect this small-scale variability to affect catchment-scale response. This is plausible if we adopt a reasoning along the lines of the central limit theorem where aggregation, in general, produces more linear and less variable response [e.g., *Sivapalan and Wood*, 1986]. The reduced uncertainty may be partly due to less nonlinear behavior at the catchment scale. The central limit theorem, however, applies to independent and identically distributed random variables. Very likely, the underlying soil variability and runoff processes are neither independent nor random, and structured heterogeneity and structured processes may dominate the system response [*Blöschl and Sivapalan*, 1995; *Western et al.*, 2001]. The analyses did indicate a state-dependent predictability at the catchment scale similar to that at the plot scale (Figure 8) and the role of the transition between matrix and macropore flow is quite apparent at the catchment scale when examining contributing areas (Figure 11). Part of this threshold effect at the catchment scale is related to the presence of two different soils with contrasting hydraulic characteristics. Different microstates of initial soil moisture may therefore produce significantly different initial soil hydraulic conductivity patterns which determine the amount of infiltration excess runoff that is generated. These analyses suggest that, as one moves from the plot to the catchment scale, part of the small-scale variability averages out but there is also an emerging source of uncertainty that is not present at the plot scale. This idea of variability averaging out and additional sources of variability becoming important when moving up in scale is consistent with the more general discussion of various hydrologic processes of *Western et al.* [2003, p.135].

[55] We believe there is an additional, and perhaps more straightforward, interpretation of the increasing predictability with scale found in this paper. The specifications of the macrostates at the plot and catchment scales in this paper are not exactly the same. At the plot scale we specified the macrostate of initial soil moisture by the first two moments of the spatial distribution derived from TDR point measurements. At the catchment scale the description of the soil moisture macrostate is more detailed than that at the plot scale as, in addition to the univariate moments, the values at individual points (through conditioning of the soil moisture realizations) and the variogram are specified. It is possible that the decrease in uncertainty with increasing scale is related to using more detailed information at the larger scale. We have argued that this is a typical setup in a research catchment as, at the plot scale, disturbances of the soil by the measurements are more problematic than at the catchment scale. As we go up in scale, often, more data will be available which may decrease the uncertainty and hence increase the predictability. It would be interesting to repeat the catchment-scale analyses of this paper and specify the first and second univariate moments only to examine whether the level of detail of the macrostate descriptions affects the predictability.

6.3. Implications for Process Studies and Modeling

[56] In this study we have put a lot of effort in realistically portraying the processes in the Weiherbach catchment in the CATFLOW model by using fairly detailed measurements at various scales. This gives us some confidence that the model does reflect the important infiltration and runoff processes at both the plot and catchment scales in a realistic way. We therefore can interpret the realizations of the Monte Carlo simulations as repeated plot-scale and catchment-scale experiments. All of these repeated experiments are identical in their macrostate of initial soil moisture as defined by what we can typically measure in a research catchment but they differ in their microstate of fine-scale soil moisture variability not captured by the monitoring network. As all these microstates belong to the same macrostate of initial soil moisture they may not be distinguished by the measurement strategy used in the field. The simulations have indicated that the response will indeed not be unique if the average initial state approaches a threshold, i.e., if nonlinearity becomes important for the system response. As a consequence, for apparently identical experimental conditions preferential flow may or may not occur, solute transport depths can vary by more than 90% and flood peaks can vary by more than 30%. These limits to predictability provide a suitable explanation for apparently inconsistent experimental results such as the tracer breakthrough velocities of *Lischeid et al.* [2000] that varied between 30.6 and 10.6 m d^{-1} for identical experimental conditions. By the same token, observed runoff response at the catchment scale is often difficult to interpret in a unique way. We believe, again, that part of this difficulty stems from the intrinsic limits to predictability given a typical set of measurements. Of course, the additional difficulty at the catchment scale is that the rainfall forcing can not usually be controlled.

[57] One would generally hope that a detailed set of field measurements would constrain the system state enough to give unique results when used for hydrologic modeling but the results of this paper suggest that this is not necessarily the case. These limits to obtaining unique relationships in experiments and observations have direct implications for model representations. *Beven* [2000, p. 211] notes that "field process studies are by their nature unique in both space and time; they cannot be repeated under exactly the same boundary and initial conditions," and he goes on to discuss the implications for modeling. One of the implications is the need to resort to calibration strategies to make models work and this is true at various scales [*Beven*, 1989; *Grayson et al.*, 1992]. It is clear that if one calibrates parameters to compensate for the real uncertainty in the microstate of initial conditions this is likely a "quick fix" which may jeopardize the realism of the model. Obviously, a much better strategy would be to allow for the uncertainty in the initial microstate rather than to seek a best fit of the model to the one realization of hydrologic response available. The soil moisture data used in this paper have been fairly detailed (50 and 61 measurement points at the plot and catchment scales, respectively). With a few exceptions [e.g., *Western and Grayson*, 1998] the number of monitoring sites will be much lower in most hydrologic studies. This means that the predictability will be lower than what has been obtained in this paper. Also, we considered a single source of uncertainty only, i.e., the initial conditions, assuming a perfect representation of the governing processes (in terms of model structure and model parameters) and assuming errors in the forcing to be small. It is clear that these

additional sources of uncertainty will degrade the predictability beyond the results of this paper.

[58] We have adopted the concepts of microstates and macrostates from statistical mechanics and think these are powerful concepts to analyze the role of measurements in modeling or, more generally, in representing reality. There is, however, an important distinction between hydrology and standard statistical mechanics. The latter deal with large aggregates that can be aggregated by statistical methods while hydrology usually deals with what *Weinberg* [1975] terms intermediate systems that cannot be aggregated easily because of their intermediate number of degrees of freedom and their complexity (see the discussion of *Dooge* [1986]). The manifestation of these two characteristics at the plot and catchment scales is the nonlinearity of hydrologic system response and the presence of organized, nonrandom variability. In this paper we have used a deterministic numerical model to examine the aggregation and error propagation effects but a more elegant approach would involve an analytical study of the limits to predictability imposed by uncertain microstates. Because of the characteristics of intermediate systems this will not be easy.

[59] The processes studied here involving a switch between matrix and macropore regimes and the threshold nature of infiltration excess runoff generation, are one particular subset of threshold processes. We believe that the results of the limits to predictability are more generally applicable to hydrologic nonlinear processes. Similar patterns of predictability can probably be expected for other threshold processes, or more generally, nonlinear processes in hydrology at various spatial and temporal scales. One example in the Weiherbach catchment is a feedback mechanism between physical and biological processes. Earthworm activity controls the dynamics of subsurface flow processes and hence soil moisture through the generation of macropores. Conversely, soil moisture controls the macropore location to some degree because of the earthworms' preference for wetter parts of the catchment. This feedback mechanism is likely to produce some very interesting nonlinearities. Numerous other feedback mechanisms, nonlinearities and threshold processes exist in hydrology which are likely to translate into domains of high and low predictability. As *NRC* [2003, p. 21] noted, among the key unresolved issues and research challenges in hydrology is "separating the predictable and the unpredictable". This paper is an initial contribution to identifying the boundaries of predictable and unpredictable domains in one particular setting and it is hoped that future research will shed more light on the patterns of predictability in more generic hydrologic contexts.

[60] **Acknowledgments.** We would like to thank the German Ministry of Education and Research for financial support of the Weiherbach project as well as Erich Plate for his thoughtful guidance of the project. We are grateful to Thomas Maurer for significant contributions to the CATFLOW model. The authors would like to thank the Austrian Science Foundation (FWF), project no. P14478-TEC, and the Austrian Academy of Sciences, project HÖ 18, for financial support. The model and the data set is freely available for academic use by email request to ezehe@rz.uni-potsdam.de.

References

Bárdossy, A., U. Haberlandt, and J. Grimm-Strele (1996), Regional scales of groundwater quality parameters and their dependence on geology and land use, in *Groundwater and Subsurface Remediation*, edited by H. Kobus, B. Barczewski, and H.-P. Koschitzky, pp. 195–204, Springer-Verlag, New York.

Beven, K. (1989), Changing ideas in hydrology—The case of physically based models, *J. Hydrol.*, *105*, 157–172.

Beven, K. J. (2000), Uniqueness of place and process representations in hydrological modeling, *Hydrol. Earth Syst. Sci.*, *4*(2), 203–213.

Beven, K. J., and M. J. Kirkby (1979), A physically-based, variable contributing area model of basin hydrology, *Hydrol. Sci. Bull.*, *24*, 43–69.

Blöschl, G. (1999), Scaling issues in snow hydrology, *Hydrol. Processes*, *13*, 2149–2175.

Blöschl, G., and M. Sivapalan (1995), Scale issues in hydrological modelling: A review, *Hydrol. Processes*, *9*, 251–290.

Blöschl, G., R. B. Grayson, and M. Sivapalan (1995), On the representative elementary area (REA) concept and its utility for distributed rainfall-runoff modeling, *Hydrol. Processes*, *9*, 313–330.

Boltzmann, L. (1995), *Lectures on Gas Theory*, translated from German by Stephen G. Brush, reprint, Dover, Mineola, N. Y.

Brooker, I. (1985), Two-dimensional simulation by turning bands, *Math. Geol.*, *17*(1), 81–90.

Celia, M. A., and E. T. Bouloutas (1990), A general mass-conservative numerical solution for the unsaturated flow equation, *Water Resour. Res.*, *26*(7), 1483–1496.

Dooge, J. C. I. (1986), Looking for hydrologic laws, *Water Resour. Res.*, *22*, 46S–58S.

Flury, M. (1996), Experimental evidence of transport of pesticides through field soils—A review, *J. Environ. Qual.*, *25*(1), 25–45.

Flury, M., H. Flühler, J. Leuenberger, and W. A. Jury (1994), Susceptibility of soils to preferential flow of water: A field study, *Water Resour. Res.*, *30*(7), 1945–1954.

Gleick, J. (1993), *Chaos, Making a New Science*, 352 pp., Abacus, London.

Grayson, R. B., and G. Bölschl (Eds.) (2000), *Spatial Patterns in Catchment Hydrology: Observations and Modelling*, 404 pp., Cambridge Univ. Press, New York.

Grayson, R. B., I. D. Moore, and T. A. McMahon (1992), Physically-based hydrologic modeling: 2. Is the concept realistic?, *Water Resour. Res.*, *28*, 2659–2666.

Grayson, R. B., G. Blöschl, and I. D. Moore (1995), Distributed parameter hydrologic modelling using vector elevation data: THALES and TAPES-C, in *Computer Models of Watershed Hydrology*, edited by V. P. Singh, pp. 669–696, Water Resour. Publ., Highlands Ranch, Colo.

Grayson, R. B., A. W. Western, F. H. S. Chiew, and G. Blöschl (1997), Preferred states in spatial soil moisture patterns: Local and non-local controls, *Water Resour. Res.*, *33*(12), pp. 2897–2908.

Landau, L. D., and E. M. Lifshitz (1999), *Statistical Physics*, *Course Theoretical Phys.*, vol. 5, Butterworth-Heinemann, Woburn, Mass.

Lennartz, B., J. Michaelsen, W. Wichtmann, and P. Windmoser (1999), Time variance analysis of preferential solute movement at a tile-drained field site, *Soil Sci. Soc. Am. J.*, *63*, 39–47.

Lischeid, G., H. Lange, and M. Hauhs (2000), Information gain using single tracers under steady state tracer and transient flow conditions: The Gårdsjön G1 multiple tracer experiments, in *Proceedings of the Tram'2000 Conference Tracers and Modelling in Hydrogeology*, *IAHS Publ.*, *262*, 73–77.

Matheron, G., and G. de Marsily (1980), Is transport in porous media always diffusive? A counter example, *Water Resources Res.*, *16*(5), 901–917.

Maurer, T. (1997), Physikalisch begründete, zeitkontinuierliche Modellierung des Wassertransports in kleinen ländlichen Einzugsgebieten, *Mitt. Inst. Hydrol. Wasserwirt. 61*, Univ. Karlsruhe, Karlsruhe, Germany.

Merz, B., and A. Bárdossy (1998), Effects of spatial variability on the rainfall runoff process in a small loess catchment, *J. Hydrol.*, *212–213*, 304–317.

Mualem, Y. (1976), A new model for predicting the hydraulic conductivity of unsaturated porous media, *Water Resour. Res.*, *12*, 513–522.

National Research Council (NRC) (2003), *Predictability and Limits-to-Prediction in Hydrologic Systems*, Natl. Acad. Press, Washington, D. C.

Roth, K., and K. Hammel (1996), Transport of a conservative chemical through an unsaturated two-dimensional miller-similar medium with steady state flow, *Water Resour. Res.*, *32*(6), 1653–1663.

Russo, D., J. Zaidel, and A. Laufer (1994), Stochastic analysis of solute transport in a partially saturated heterogeneous soil: 1. Numerical experiments, *Water Resour. Res.*, *30*(3), 769–779.

Schäfer, D. (1999), Bodenhydraulische Funktionen eines Kleineinzugsgebiets—Vergleich und Bewertung unterschiedlicher Verfahren, Ph.D. dissertation, Inst. of Hydromech., Univ. of Karlsruhe, Karlsruhe, Germany.

Sivakumar, B. (2000), Chaos theory in hydrology important issues and interpretations, *J. Hydrol.*, *227*, 1–20.

Sivapalan, M., and E. F. Wood (1986), Spatial heterogeneity and scale in the infiltration response of catchments, in *Scale Problems in Hydrology*, edited by V. K. Gupta. I. Rodríguez-Iturbe, and E. F. Wood, pp. 81–106, D. Reidel Publ., Norwell, Mass.

Tolman, R. C. (1979), *The Principles of Statistical Mechanics*, reprint, Dover, Mineola, N. Y.

Tsang, Y. W., C. F. Tsang, F. Hale, and V. B. Dverstorp (1996), Tracer transport in a stochastic continuum model, *Water Resour. Res.*, *32*(10), 3077–3092.

van Genuchten, M. T. (1980), A closed-form equation for predicting the hydraulic conductivity of unsaturated soils, *Soil Sci. Soc. Am. J.*, *44*, 892–898.

Villholth, K., K. Jensen, and J. Frederica (1998), Flow and transport processes in a macroporous subsurface-drained glacial till soil: I. Field investigation, *J. Hydrol.*, *207*, 98–120.

Webb, E. K., and M. P. Anderson (1996), Simulation of preferential flow in three dimensional heterogeneous conductivity fields with realistic internal architecture, *Water Resour. Res.*, *32*(3), 533–545.

Weinberg, G. M. (1975), *An Introduction to General Systems Thinking*, 279 pp., John Wiley, Hoboken, N. J.

Western, A. W., and G. Blöschl (1999), On the spatial scaling of soil moisture, *J. Hydrol.*, *217*, 203–224.

Western, A. W., and R. B. Grayson (1998), The Tarrawarra data set: Soil moisture patterns, soil characteristics, and hydrological flux measurements, *Water Resour. Res.*, *34*(10), 2765–2768.

Western, A. W., G. Blöschl, and R. B. Grayson (2001), Toward capturing hydrological significant connectivity in spatial patterns, *Water Resour. Res.*, *37*(1), 83–97.

Western, A., R. Grayson, and G. Blöschl (2002), Scaling of soil moisture: A hydrologic perspective, *Annu. Rev. Earth Planet. Sci.*, *30*, 149–180.

Western, A. W., R. B. Grayson, G. Blöschl, and D. J. Wilson (2003), Spatial variability of soil moisture and its implications for scaling, in *Scaling Methods in Soil Physics*, edited by Y. A. Perchepsky, H. M. Selim, and D. E. Radcliffe, pp. 120–142, CRC Press, Boca Raton, Fla.

Wood, E. F. (1976), An analysis of the effects of parameter uncertainty in deterministic hydrologic models, *Water Resour. Res.*, *12*(5), 925–932.

Wood, E. F., M. Sivapalan, K. Beven, and L. Band (1988), Effects of spatial variability and scale with implications to hydrologic modeling, *J. Hydrol.*, *102*, 29–47.

Zehe, E. (1999), Stofftransport in der ungesättigten Bodenzone auf verschiedenen Skalen, Ph.D. dissertation, Univ. of Karlsruhe, Karlsruhe, Germany.

Zehe, E., and H. Flühler (2001a), Preferential transport of isoproturon at a plot scale and a field scale tile-drained site, *J. Hydrol.*, *247*, 100–115.

Zehe, E., and H. Flühler (2001b), Slope scale variation of flow patterns in soil profiles, *J. Hydrol.*, *247*, 116–132.

Zehe, E., T. Maurer, J. Ihringer, and E. Plate (2001), Modelling water flow and mass transport in a Loess catchment, *Phys. Chem. Earth B*, *26*(7–8), 487–507.

Zurmühl, T., and W. Durner (1996), Modelling transient water flow and solute transport in a biporous soil, *Water Resour. Res.*, *32*(4), 819–829.

G. Blöschl, Institute of Hydraulics, Hydrology and Water Resources Management, Vienna University of Technology, A-1040 Vienna, Austria.

E. Zehe, Institute of Geoecology, University of Potsdam, 14415 Potsdam, Germany. (zehe@iws.uni-stuttgart.de)